Paired and solitary ionocytes in the zebrafish olfactory epithelium

Julia Peloggia[1,*], King Yee Cheung[2,3,*], Tanya T. Whitfield[3,^], Mariela D. Petkova[4], Richard Schalek[4], Jonathan Boulanger-Weill[4,5], Yuelong Wu[4], Shuohong Wang[4], Nicholas J. van Hateren[3], Michał Januszewski[6], Viren Jain[7], Jeff W. Lichtman[4], Florian Engert[4], Tatjana Piotrowski[1] and Suresh Jesuthasan[2,8,^].

*equal contribution

^corresponding authors: t.whitfield@sheffield.ac.uk, suresh.jesuthasan@umu.se

[1]Stowers Institute for Medical Research, Kansas City, MO 64110, USA.

[2]Lee Kong Chian School of Medicine, Nanyang Technological University, Singapore 636921.

[3]School of Biosciences, Bateson Centre and Neuroscience Institute, University of Sheffield, Sheffield, S10 2TN, United Kingdom.

[4]Department of Molecular and Cellular Biology, Center for Brain Science, Harvard University, Cambridge, MA 02138, USA.

[5]Sorbonne Université, Institut National de la Santé et de la Recherche Médicale, Centre National de la Recherche Scientifique, Institut de la Vision, Paris, France

[6]Google Research, Zürich 8002, Switzerland.

[7]Google Research, Mountain View, CA 94043, USA.

[8]Department of Molecular Biology, Umeå University, Sweden.

Short title: Gene expression and morphology of zebrafish olfactory ionocytes

Abstract

The sense of smell is generated by electrical currents that are influenced by the concentration of ions in olfactory sensory neurons and mucus. In contrast to the extensive morphological and molecular characterization of sensory neurons, there has been little description of the cells that control ion concentrations in the zebrafish olfactory system. Here, we report the molecular and ultrastructural characterization of zebrafish olfactory ionocytes. Transcriptome analysis suggests that the zebrafish olfactory epithelium contains at least three different ionocyte types, which resemble Na^+/K^+-ATPase-rich (NaR), Na^+/Cl^- cotransporter (NCC), and H^+-ATPase-rich (HR) cells, responsible for calcium, chloride, and pH regulation, respectively, in the zebrafish skin. NaR-like and HR-like ionocytes are usually adjacent to one another, whereas NCC-like cells are usually solitary. The distinct subtypes are differentially distributed: NaR-like/HR-like cell pairs are found broadly within the olfactory epithelium, whereas NCC-like cells reside within the peripheral non-sensory multiciliated cell zone. Comparison of gene expression and serial-section electron microscopy analysis indicates that the NaR-like cells wrap around the HR-like cells and are connected to them by shallow tight junctions. The development of olfactory ionocyte subtypes is also differentially regulated, as pharmacological Notch inhibition leads to a loss of NaR-like and HR-like cells, but does not affect NCC-like ionocyte number. These results provide a molecular and anatomical characterization of olfactory ionocytes in a stenohaline freshwater teleost. The paired ionocytes suggest that both transcellular and paracellular transport regulate ion concentrations in the olfactory epithelium, while the solitary ionocytes may enable independent regulation of multiciliated cells.

Introduction

Olfaction is mediated by a combination of ion currents – an influx of calcium followed by an efflux of chloride – that is triggered by the binding of an odorant to its receptor on olfactory sensory neurons (OSNs) [1,2]. The high concentration of chloride in the dendritic knobs and cilia of mammalian OSNs is achieved by uptake from the mucus by the NKCC1 (Slc12a2) co-transporter, which requires external sodium [3]. Despite the relative robustness of transduction that is offered by the chloride current [4], olfactory sensitivity is influenced by external ion concentrations [5]. The zebrafish, a freshwater fish that can be found in the wild in water with a moderate range of salinity [6], has provided fundamental insights into olfactory processing [7,8]. The morphological and molecular features of OSNs of this animal are well described [9–11]. However, it is unclear how ion composition in the zebrafish olfactory epithelium is regulated.

Ionocytes are mitochondria-rich cells that can transport ions intracellularly against their concentration gradient. In freshwater teleosts, ionocytes in the skin and gills actively absorb ions from the external environment, compensating for passive water gain (reviewed in [12,13]). In marine teleosts, ionocytes in the kidneys and gills actively secrete excess ions absorbed from seawater. Recently, with the advent of single cell sequencing technologies, ionocytes have been identified based on gene expression in several tissues including the olfactory epithelium in humans and mice [14,15], inner ear of mice [16] and the lateral line neuromasts in zebrafish [17]. In the neuromasts, as in the gill and skin of fish, a subset of ionocytes were found in a complex; the presence of shallow tight junctions in such complexes [18] is thought to provide an alternative paracellular pathway for ion movement, for example by coupling Na^+ secretion to Cl^- efflux via the CFTR (cystic fibrosis transmembrane

conductance regulator) channel in an adjacent ionocyte in the gill of *Fundulus* in seawater [19] .

The existence of ionocytes in the olfactory epithelium of fish was first suggested in 1972 based on light and electron microscopy of Baltic Sea trout [20]. The cells, termed “labyrinth cells”, were characterised by an abundance of mitochondria as well as smooth endoplasmic reticulum, and were proposed to be functionally equivalent to “chloride cells” in the gill. A transmission electron microscopy (TEM) and scanning electron microscopy (SEM) study in 2001 confirmed the presence of cells with a similar appearance in the olfactory epithelium of seven freshwater fish species, and noted their distinct morphology: an apical surface with microvilli-like projections and occasional invaginations of the cell membrane [21]. Labyrinth cells were also recently identified in the freshwater goby, where they were described as having a globular appearance in scanning electron micrographs [22]. However, little is known about the molecular characteristics of these putative ionocytes, and it is not known if they exist in isolation or as complexes.

In mammals and frogs, the winged helix/forkhead transcription factor Foxi1 is required for ionocyte specification, and thus provides a useful marker for ionocytes. In zebrafish, the Foxi1 orthologs *foxi3a* and *foxi3b* regulate ionocyte development, and loss of *foxi3a* leads to complete loss of ionocytes [23,24]. Based on their *foxi3a* expression, several classes of epidermal and gill ionocytes in the zebrafish were discovered, including: H^+-ATPase-rich (HR) ionocytes which secrete protons, take up sodium, and excrete ammonium ions; Na^+/-K^+-ATPase-rich (NaR) ionocytes which take up calcium ions; Na^+/Cl^- co-transporter-expressing (NCC) ionocytes which take up sodium and chloride ions; and K^+-secreting (KS) ionocytes which secrete potassium ions (reviewed in [12,13,25]). The different classes of ionocytes possess

distinct gene expression profiles [13,17]; distinguishing markers include *trpv6* (for NaR [26]), *ceacam1* (for HR [27]), and *slc12a10.2* (for NCC [28,29]). Here, we use transcriptomic data, in situ hybridization and serial-section electron microscopy (ssEM) to characterise the different subtypes of ionocytes in the zebrafish olfactory epithelium.

Results

Single-cell RNA sequencing reveals the presence of several classes of olfactory ionocytes

To search for potential ionocytes in the zebrafish olfactory epithelium, we used single-cell RNA sequencing (scRNA-seq) datasets generated from dissected adult olfactory rosettes [30]. We identified both major types of olfactory sensory neurons (OSNs; ciliated and microvillous, marked by *ompb* and *trpc2b*, respectively), supporting cells, neuronal progenitors and immune cell clusters (Fig. 1A, S1A–C). Additionally, we found a cluster containing the well-conserved pan-ionocyte markers, *foxi3a* and *foxi3b* [23,24]. Differential gene expression among clusters shows the expression of NaR ionocyte genes such as *trpv6*, *gcm2*, *fxyd11* (*si:dkey-33i11.4*) [31] and *atp1a1a.3* [32], and HR ionocyte markers, such as *ceacam1* (Fig. 1B–F; cluster 18 in Table S1). The cluster contains a high level of mitochondrial genes (Fig. S1D), consistent with the mitochondria-rich characteristic of ionocytes. We did not detect genes characteristic of other zebrafish ionocyte subtypes, such as *slc12a10.2* [28]. Differential expression analysis also indicated the expression of genes mediating Notch-Delta signalling (e.g. *lfng*, *notch1b*), similar to what has been described in

different ionocyte subtypes [17,33]. These results suggest the presence of olfactory ionocytes in the adult zebrafish.

To determine if olfactory ionocytes are present at larval stages, we searched for the expression of ionocyte marker genes in scRNA-seq datasets from larval zebrafish [34,35]. In addition to the expression in previously defined ionocyte clusters, we found that the same genes were co-expressed in a small group of cells within the larval olfactory epithelium cluster (Fig. 1H,I). Interestingly, in a separate dataset from larval epithelial cells [17], we detected *foxi3b*$^{+}$ cells in the olfactory epithelium cluster that do not express genes that mark NaR and HR cells. Differential gene expression of these *foxi3b*$^{+}$ cells against the remaining cells revealed a different set of ionocyte markers, including *slc12a10.2*, characteristic of NCC ionocytes (Fig. 1J–M; Table S2).

Transcriptomic data thus suggest the presence of three distinct subtypes of ionocytes in the larval olfactory epithelium and adult zebrafish olfactory rosette. These subtypes have transcriptional signatures of skin NaR, HR and NCC ionocytes.

Spatial expression analysis identifies paired and solitary olfactory ionocytes

To validate the transcriptomic data, and to determine the localization and number of olfactory ionocytes in larval fish, we performed whole-mount fluorescent in situ hybridization with hybridization chain reaction (HCR RNA-FISH) [36]. We initially examined the expression of *foxi3b*, expressed in all ionocyte subtypes detected in the olfactory transcriptomes, and *trpv6* and *ceacam1* to label the NaR and HR ionocyte populations, respectively. *foxi3b*$^{+}$ cells were found in all regions of the olfactory pit at 5 days post-fertilization (dpf), but were enriched in the postero-lateral

region (see white arrowhead; Fig. 2A–A'). There was a mean of 21 *foxi3b*$^{+}$ cells per olfactory pit (*N* of olfactory pits = 6).

A subset of the *foxi3b*$^{+}$ cells expressed the HR marker *ceacam1* (Fig. 2B). Interestingly, we always detected one *ceacam1*$^{+}$ (HR-like) cell adjacent to a *trpv6*$^{+}$ (NaR-like) cell (Fig. 2A–A'',C–C''). These pairs of cells typically had nuclei situated deep in the epithelium, and each had an extension reaching the epithelial surface (see magenta and cyan arrowheads, Fig. 2C; Movie S1). Notch pathway genes are expressed in olfactory ionocytes (Fig. 1B). To test whether Notch signalling is active in these pairs, we used the Notch reporter *Tg(tp1bglobin:EGFP)*^{um14} in combination with HCR RNA-FISH. Notch signalling is active in one of the two cells of the ionocyte pairs in the olfactory epithelium, with the NaR-like ionocyte (*trpv6*$^{+}$) being the Notch-positive cell of the pair (Fig. 2D–D'').

To test which other ion channel genes are expressed in these cells, we performed additional stainings for HR markers. Indeed, the *trpv6*$^{-}$ cell of the pair expresses the sodium/proton transporter *slc9a3.2* (Fig. 2E) and the anion transporter *slc4a1b* (Fig. 2F). However, these cells do not express the ammonium transporter *rhcgb* (Fig. S2), which has been detected in HR ionocytes in the skin [37].

Besides the presence of *trpv6*$^{+}$ and *ceacam1*$^{+}$ ionocyte pairs, we also observed solitary *foxi3b*$^{+}$ cells that were not paired with *ceacam1*$^{+}$ cells (Fig. 2C). These cells were positioned on the lateral borders of the olfactory pit and had a rounded morphology (see yellow arrowhead, Fig. 2C; Movie S2). To test if these *foxi3b*$^{+}$ cells correspond to the NCC-like cells present in the larval epithelial dataset, we performed HCR RNA-FISH, combining a *foxi3b* probe with different markers obtained from differential expression analysis of scRNA-seq data. We confirmed that

these solitary *foxi3b*$^+$ cells express the NCC ionocyte markers *slc12a10.2, chrd* and *hepacam2* [14,17] (Fig. 2G–I).

We used HCR RNA-FISH to examine the distribution of ionocytes in adult zebrafish olfactory rosettes. Ionocyte pairs were detected throughout the rosette (Fig. 3A–B'''); *trpv6*$^+$ cells were adjacent to a strongly *ceacam1*$^+$ cell throughout the epithelium, with both cell types having varying levels of *foxi3b* expression (Fig. 3B''',C''',D'''). In the peripheral non-sensory region, by contrast, we additionally observed *foxi3b*$^+$ cells with no expression of *trpv6* or *ceacam1* (Fig. 3C–E'''). These NCC-like ionocytes appeared rounded in all cases (Fig 3D,D''',E,E'''; Fig. S3), whereas NaR-like/HR-like ionocytes had variable morphologies, appearing elongated in the region close to the OSN zone, and rounded in the most peripheral non-sensory regions (Fig. 3D–E''').

We conclude that the zebrafish olfactory epithelium contains three main types of ionocytes, at both larval and adult stages. One type is an NCC-like ionocyte, which is solitary and expresses the chloride channel *slc12a10.2*. The other two types, which are present in pairs, consist of one *trpv6*$^+$, NaR-like ionocyte and one *ceacam*$^+$, HR-like ionocyte.

Time-course of olfactory ionocyte development

To determine when olfactory ionocytes appear during embryonic development and their dynamics, we performed a time course analysis of *foxi3b* and *trpv6* expression from 1 to 5 dpf (Fig. 4). None of the ionocyte subtypes were observed in embryos at 1 dpf. Most olfactory pits showed solitary *foxi3b*$^+$ ionocytes at 2 dpf, while paired ionocytes were not as frequent (Fig. 4A,B). The numbers of all olfactory ionocyte subtypes progressively increased over time (Fig. 4A–C).

Besides the presence of mature ionocytes, we also detected *foxi3a*$^{+}$ cells adjacent to the olfactory epithelium (Fig. S4A). These cells did not express any of the ion channel genes we examined by HCR RNA-FISH. Similar cells have been observed in the lateral line neuromast [17]. In these organs, neuromast ionocyte progenitors are *krt1-19e*$^{+}$ skin cells which turn off expression of the ionocyte specification transcription factor genes *foxi3a* and *foxi3b* as they invade neuromasts, where they differentiate. To test if *krt1-19e*$^{+}$ cells give rise to new ionocytes in the olfactory epithelium during development, we performed time-lapse analyses of the transgenic line *Tg(krtt1c19e:lyn-tdTomato)*^{sq16}. While we observed several new ionocytes invading the lateral line neuromasts, we did not observe any *tdTomato*$^{+}$ cells migrate into the olfactory pit (Fig. S2B,C; Movie S3). Additionally, olfactory pits did not contain any *tdTomato*$^{+}$ cells, suggesting that these cells do not give rise to ionocytes in the olfactory epithelium (Fig. S2B,C''). We cannot distinguish, however, whether olfactory ionocytes are derived from *krt1-19e*$^{-}$ basal cells or if the transgenic line does not label the population of basal cells surrounding the olfactory epithelium.

Notch signalling differentially regulates olfactory ionocyte number

Ionocyte differentiation and survival is regulated by Notch signalling in different tissues [17,24,33]. To test if Notch signalling also plays a role in ionocyte development and maintenance in the olfactory epithelium, we treated 4 dpf larvae for 24h with the gamma-secretase inhibitor LY411575, which inhibits Notch signalling (Fig. 5A). We observed a striking loss of NaR- and HR-like pairs, but no change to NCC-like ionocyte number in the olfactory epithelium (Fig. 5B–E). The remaining NaR- and HR-like pairs show altered cell morphology, and could be undergoing cell death (Fig. 5E).

In neuromast (Nm) ionocytes, transcription of the Notch ligand gene *dld* is upregulated during division of the ionocyte progenitor cell into the NaR- and HR-like pair, resulting in two *dld*$^{+}$ cells [17]. To investigate whether olfactory NaR- and HR-like pairs develop in a similar manner, we performed time-lapse analysis of the transgenic *dld* reporter line *Tg(dld:hist2h2l-EGFP)*^{psi84Tg} from 3–5 dpf. We observed pairs of EGFP+ cells appear at the edge of the pit, upregulate EGFP and differentiate into ionocytes (Movies S4, S5). These data suggest that, similar to Nm ionocytes, NaR- and HR-like ionocyte pairs in the olfactory epithelium do not originate from the division of pre-existing ionocyte pairs, but come from a different population of progenitor cells.

Ultrastructure of larval zebrafish olfactory ionocytes

To describe the ultrastructure and three-dimensional shape of olfactory ionocytes, we examined a serial-section electron microscopy (ssEM) dataset of a 7 dpf wild-type zebrafish larva. Here, we found mitochondria-rich cells in the olfactory epithelium with ultrastructural features typical of teleost ionocytes [20,21,38–41]. An extensive tubular network gave the cytoplasm a lacy appearance, quite distinct from that of OSNs or other olfactory cell types, making it possible to spot these relatively rare cell types. Consistent with the HCR RNA-fish data, the cells had differing shape and appearance in different regions of the olfactory epithelium.

We found several examples of ionocytes within the OSN zone of the olfactory pit (Fig. 6). These slender cells spanned almost the full width of the epithelium (>20 µm in apicobasal length), with nuclei positioned just above basal cells near the basal lamina. In line with the transcriptomics data, most examples consisted of a pair of cells. One member of the pair, which we propose is the HR-like cell (see below), terminated in an apical knob bearing ~50 short, irregular microvilli, intermediate in

diameter (0.2 µm) between the microvilli of microvillous OSNs (0.1 µm diameter) and the cilia of ciliated OSNs and non-sensory multiciliated cells (MCCs; 0.25–0.3 µm diameter) (Fig. 6A,C,E,E'). Apart from a cortical zone at the cell apex, the cytoplasm was densely packed with mitochondria in close association with an extensive intracellular tubular network (Fig. 6C,D).

The HR-like ionocytes within the OSN zone were closely associated with a second cell along most of their apicobasal length (Fig. 6). This second cell wrapped around the HR-like ionocyte at the cell apex with a thin layer of cytoplasm, forming a crescent in transverse section (Fig. 6A–E'''). At their apices, the two cells were connected with a continuous shallow (0.1–0.2 µm) tight junction (zonula occludens), and to surrounding cells with deep (0.5–1 µm) tight junctions (Fig. 6F,G,L). In a gap not covered by the wrapping cell, the ionocyte was sealed to an olfactory supporting cell by a deep tight junction (Fig. 6F,G). The cytoplasm of the wrapping cell also had some ionocyte-like characteristics (e.g. some tubules and pores). The ultrastructure of both cells of the pair was clearly distinct from the supporting cells that surround and insulate the OSNs, which are full of secretory granules (Fig. 6C).

To determine which member of the cell pair corresponded to which type of ionocyte, we compared the morphology of the ssEM 3D reconstructions to that of live cells imaged at 5 dpf with the *Tg(tp1bglobin:EGFP)* Notch reporter line, which marks the NaR-like ionocytes (Fig. 6H–K). The morphology of the live NaR-like cells clearly matched that of the wrapping cells seen in the ssEM dataset, with a thin curved layer of cytoplasm near the cell apex, sometimes appearing as a doublet in lateral view (Fig. 6H,H'), and forming a clear crescent in a top-down view (Fig. 6K). Taken together, the ssEM and fluorescence imaging data strongly suggest that the ionocyte cell pairs found in the ssEM dataset correspond to the HR-like and NaR-like ionocyte

pairs identified through transcriptomic profiling, with the NaR-like cell wrapping around the apex of the HR-like cell.

We also found occasional examples of multicellular ionocyte complexes consisting of three or four cells within the OSN zone of the larval olfactory epithelium (Fig. 6L–S). In one example (Fig. 6L–P), one HR-like/NaR-like pair was associated with a second possible NaR-like cell. In this example, the HR-like ionocyte was closely associated with a ciliated OSN at its base. In another example (Fig. 6Q), the cell complex appeared to consist of an HR-like/NaR-like pair with a second possible HR-like cell. We also found a four-cell complex consisting of a pair of HR-like/NaR-like pairs, separate at their apices, but closely associated beneath the surface of the epithelium (Fig. 6R,S).

Olfactory ionocytes with a different morphology were present in the MCC zone at the periphery of the olfactory pit (Fig. 7). Here, the rounded microvillous apical knobs of individual ionocytes could be identified by scanning electron microscopy (SEM) in *ift88*$^{-/-}$ mutant larvae at 4 dpf (Fig. 7A–C). These mutants lack cilia, which would otherwise obscure these cells in the wild type. Ionocytes were visible in the olfactory pits of two out of three individuals. In the ssEM dataset of a wild-type larva at 7 dpf, mitochondria-rich cells containing a dense tubular network were present within the non-sensory zone of MCCs (Fig. 7D–M). Some of these peripheral ionocytes were cuboidal in shape, without the long narrow neck of the ionocytes in the central OSN zone, where the olfactory epithelium is thicker (Fig. 7D–I). Other ionocytes in the MCC zone were more columnar in shape (Fig. 7J). Peripheral ionocytes formed deep tight junctions with surrounding non-sensory MCCs, skin cells, and other ionocytes. Basally, they were positioned just above the basal cells of the olfactory epithelium (Fig. 7F,J), occasionally extending thin end-feet to contact

the basal lamina directly (Fig. 7M). However, they did not appear to be paired with, or wrapped by, any other cell along their entire apicobasal length, in contrast to the ionocytes in the OSN zone. Some, but not all, peripheral ionocytes had a large apical knob bearing ~100 irregular microvilli, with part protruding from the epithelium (Fig. 7D,F), and part sunken to form a crypt or pit (Fig. 7G), matching the morphology revealed by SEM at 4 dpf (Fig. 7C). Based on their location in the MCC zone and morphology, and in comparison to the scRNA-seq data, we identify the cuboidal peripheral olfactory ionocytes as NCC-like cells.

Discussion

Through analysis of single-cell transcriptomic, gene expression and volume electron microscopy data, we have identified at least three subtypes of ionocytes in the larval and adult zebrafish olfactory epithelium (Fig. 8). All three express the pan-ionocyte marker *foxi3b*, but can be distinguished by transcriptomic signatures and morphology. NaR-like ionocytes, expressing *trpv6*, were paired with HR-like ionocytes, expressing *ceacam1* and the transporter genes *slc9a3.2* and *slc4a1b*. NaR-like/HR-like cell pairs were situated throughout the olfactory epithelium, including within sensory regions, with cell nuclei deep in the epithelium and a long protrusion extending to the epithelial surface. NCC-like ionocytes, expressing *slc12a10.2*, *chrd*, and *hepacam2*, were located exclusively in the multiciliated cell zone of the larval olfactory pit, posterolaterally distributed, and more rounded in shape. Solitary ionocytes lacking *trpv6* and *ceacam1* were also seen in the non-sensory regions of the adult rosette. These observations suggest a complex mechanism for ion regulation throughout the zebrafish olfactory epithelium, involving region-specific roles for different ionocyte types.

Pairing of NaR-like and HR-like ionocytes may extend functionality

The pairing of NaR-like and HR-like ionocytes in the olfactory epithelium appears robust. The cells are connected to each other by specialised tight junctions and are dependent on Notch signalling for survival. The existence of ionocytes in pairs or complexes is well established, for example in the gills and skin of stenohaline saltwater fish [42,43], euryhaline fish adapted to seawater [19,44–48], and in stenohaline freshwater teleosts [49]. Pairs were also seen in the skin of the euryhaline medaka, when reared in freshwater [50]. In these cases, however, one member of the pair was termed an accessory cell. Although accessory cells have some features of ionocytes – they are mitochondria-rich, for example – they have been considered to be immature or dormant [42] or specific to seawater fish [45]. The data here, and in the neuromast [17], indicate that both members of a pair in the freshwater zebrafish are *bona fide* ionocytes.

The conservation of architecture across evolutionarily diverse fish species suggests a functional advantage in using pairs. One consequence of ionocyte pairing is the creation of a paracellular pathway that is regulated by both members of the pair. In the olfactory epithelium, the apical half of the NaR-like cell wraps around the HR-like cell, forming a paracellular pathway in the space between the two cells. Both members of the pair extend from just above the basal lamina to the surface within the sensory zone. Here, it is possible that the ionocyte pairs directly regulate ion concentration within the mucus and epithelium to optimise olfactory transduction. For example, one possible role could be to enable uptake of Cl^- after a neuronal signalling event, with apical uptake and basal secretion of Na^+ by NaR-like and HR-like ionocytes providing the driving force. This would supplement Cl^- uptake by dendrites of the sensory neurons. NaR-like/HR-like ionocyte pairs are also found in

the zebrafish neuromast [17], which contains sensory hair cells that—like OSNs—signal with a chloride efflux [51]. Thus, this specific pair may enable transport of ions that is required for this mode of signalling.

NCC-like olfactory ionocytes are located in non-sensory regions containing motile cilia

NCC-like ionocytes are strikingly different from NaR-like and HR-like ionocytes in a number of respects. In the larval and adult olfactory epithelium, NCC-like ionocytes appear to be restricted to non-sensory regions. Here, they are interspersed among multiciliated cells, which contain motile cilia that drive water into the olfactory pit [52,53]. By contrast, NCC ionocytes are absent from the zebrafish neuromast, which lack motile cilia. A close association between ionocytes and motile cilia has been observed in the skin of *Xenopus tropicalis*, where depletion of ionocytes disrupts ciliary beating [54]. In the mammalian airway, ciliary beat is regulated by intracellular chloride levels [55,56]. These observations raise the possibility that NCC-like ionocytes function specifically to influence ciliary beating in the zebrafish olfactory epithelium, which in turn shapes the detection of odorants [53].

Shared and unique properties of zebrafish olfactory ionocytes

In mammals, Foxi1^{+} ionocytes have been identified in various tissues including the kidney [57], airway epithelium [58,59], inner ear [16], salivary gland [60] and thymus [61]. These ionocytes, which are critical to function, display a number of tissue-specific properties, including type of transporters expressed and morphology. Tissue-specific gene expression in zebrafish ionocytes is illustrated by the larval transcriptome: olfactory ionocytes cluster with olfactory epithelial cells, rather than skin ionocytes. The clustering of ionocytes within their tissue of residency indicates

that they share a transcriptional signature with the cells they regulate. Some of these genes are likely to code for adhesion molecules, which are highly enriched in all ionocyte transcriptomes that we have analysed thus far. Other genes may be involved in cell-cell communication and cell signalling pathways.

In summary, this study has yielded two unexpected features of ionocytes in the zebrafish olfactory epithelium. Firstly, the epithelium contains pairs of NaR-like/HR-like ionocytes, implying that synergy between these ionocyte types is essential for maintaining ion balance. Secondly, NCC-like ionocytes are restricted to non-sensory regions, implying a distinct function in the regulation of motile cilia. Ionocytes thus have diverse roles in enabling optimal olfaction.

Materials and Methods

Zebrafish husbandry

Zebrafish strains used in this study were AB and ABTL strain wild types, *nacre* (*mitfa*$^{-/-}$) [62], *oval* (*ift88*^{tz288b}) [63], *Tg(tp1bglobin:EGFP)*^{um14} [64], *Tg(krtt1c19e:lyn-tdTomato)*^{sq16} [65], *Tg(dld:hist2h2l-EGFP)*^{psi84} [30], and *Tg(-8.0cldnb:lyn-EGFP)*^{zf106Tg} [66]. Adult zebrafish were kept on a 10-hour dark/14-hour light cycle at 28.5°C and spawned by pair-mating or marbling. Eggs were collected and staged according to standard protocols, and raised either in 0.5× embryo E2 medium (7.5 mM NaCl, 0.25 mM KCl, 0.5 mM $MgSO_4$, 75 mM KH_2PO_4, 25 mM Na_2HPO_4, 0.5 mM $CaCl_2$, 0.5 mg/L $NaHCO_3$, pH = 7.4) or 1× E3 medium (5 mM NaCl, 0.17 mM KCl, 0.33 mM $CaCl_2$, 0.33 mM $MgSO_4$, with 0.0001% methylene blue at early stages) at 28.5°C. Larvae were anaesthetised with 0.5 mM tricaine methanesulfonate (MS222) at pH 7.

Dissection of adult olfactory organs

Adult ABTL wild-type strain zebrafish were culled on ice and fixed in 4% paraformaldehyde (PFA) in 1× phosphate-buffered saline (PBS) overnight at 4°C. Adult zebrafish were transferred to a SYLGARD 184-coated (Dow Corning) Petri dish containing PBS, and olfactory organs were dissected out using Dumont #5SF forceps (Fine Science Tools). Olfactory organs were washed in PBS before proceeding with staining protocols.

Single-cell RNA sequencing (scRNA-seq) analysis

Analysis was carried out on published datasets generated from dissected adult zebrafish olfactory organs [30]. All four PBS-treated datasets were downloaded with sratoolkit (version 3.1.1). Reads were de-multiplexed and aligned to version Ensembl GRCz11 (danRer11.Ens_106) of the zebrafish genome using the CellRanger (version 7.1.0) pipeline. Subsequent analysis of the UMI count matrix was performed using Seurat (version 5.1.0) [67–71] in R version 4.3.3. Initial quality control filtered out genes expressed in fewer than three cells and cells with fewer than 200 genes. Further quality control was performed to exclude cells with more than 20000 UMIs or more than 10% mitochondrial content. The four resulting Seurat objects were combined with the function *merge()*, and cluster markers were identified with the function *FindAllMarkers()*. Dimensional reduction was performed (UMAP), and final clusters were obtained with 30 dimensions and resolution of 0.5.

Daniocell data were downloaded from the taste/olfactory subset [34]; no additional processing or clustering was performed. Ionocytes were identified based on their expression of *foxi3b*. For solitary ionocytes, a dataset from larvae was used. Olfactory epithelial cells were subset based on cluster expressions of *ompb* and

trpc2a/2b. Solitary olfactory ionocytes were then identified and manually clustered based on their *foxi3b* expression, using the function subset (object, subset = *foxi3b* > 0). Markers were then subsequently identified with the function *FindAllMarkers()*. Feature plots for all datasets were made with the function *FeaturePlot_scCustom()* from the package scCustomize.

Hybridization chain reaction RNA-fluorescence *in situ* hybridization (HCR RNA-FISH)

HCR RNA-FISH was performed on 5 dpf stage *nacre* wild-type or *Tg(tp1bglobin:EGFP)* transgenic larvae following "HCR RNA-FISH protocol for whole-mount zebrafish embryos and larvae (*Danio rerio*)" provided by Molecular Instruments or adapted with acetone-based permeabilization [17]. The probe sets used in this project were *ceacam1*-B1 (accession #: NM_001113794), *trpv6*-B1 and B2 (accession #: NM_001001849), *foxi3a*-B2 (accession #: NM_198917.2), *foxi3b*-B3 and B4 (accession #: NM_198918), *slc12a10.2*-B1 (accession #: NM_001045001.1), *slc4a1b*-B1 (accession #: NM_001168266.1), *slc9a3.2*-B4 (accession #: NM_001113479.1), *chrd*-B2 (accession #: NM_130973.3), and *hepacam2*-B2 (accession #: NM_001245085.1). The amplifiers used were B1-488, B1-647, B2-546, B2-594, B3-546, B3-647, and B4-488 (Molecular Instruments). All samples were stored in PBS at 4°C before imaging. The above standard HCR RNA-FISH protocol for larvae was modified for staining on dissected olfactory organs of adult ABTL fish. The proteinase K treatment step was adjusted to incubation in 30 µg/ml of proteinase K for 30 minutes. The remainder of the protocol remained the same.

Confocal imaging

Fixed zebrafish larvae and olfactory organs were mounted in 1–2% low melting point (LMP) agarose in PBS in glass-bottomed dishes, with larvae mounted in a dorsal view. Samples were imaged on either a Zeiss LSM 800 attached to an upright microscope with a W Plan Apochromat 40×/1.0 DIC M27 water dipping objective, a Zeiss LSM 880 Airyscan confocal microscope equipped with a Plan-Apochromat 20×/0.8 M27 air objective, a Zeiss LSM 980 Airyscan2 confocal microscope equipped with a Plan-Apochromat 10x/0.45 air objective and an LCI Plan-Apochromat 40x/1.2 water objective acquired in Airyscan SR-4Y mode, or a Nikon Ti2 Yokogawa CSU-W1 spinning disk head equipped with a Hamamatsu Orca Fusion sCMOS. Objective lenses used on the Nikon microscope were CFI Apo LWD 40× WI 1.15 NA Lambda S and CFI Apo 20× WI 0.95 NA Lambda S. The laser lines used on the Zeiss microscopes were 488, 561, 568, 633, and 647 nm. A Nikon LUNV solid state laser launch was used for lasers 395/405, 488, 561 and 647 nm for GFP/Alexa488, RFP/Alexa546, and Alexa647 respectively. Emission filters used on the Nikon were 480/30, 535/30, 605/52. Nikon Elements Advanced Research v5.41.02 (Nikon) was used for image acquisition.

Lineage tracing

Tg(krtt1c19e:lyn-Tomato)^{sq16} and *Tg(dld:hist2h2l-EGFP)*^{psi84} 3–5 dpf larvae were anaesthetised with buffered MS222 up to 150 mg/L and mounted in glass bottom dishes (Cellvis) using 0.8% low melting point agarose dissolved in DI water supplemented with buffered MS222 (120 mg/L). Time lapses were acquired in a Nikon Ti2 Yokogawa CSU-W1 spinning disk head equipped with a Hamamatsu Orca Fusion sCMOS and CFI Apo LWD 40× WI 1.15 NA Lambda S objective. A Stage Top Incubator (OkoLab) was used to keep the constant temperature of 28.5˚C and 85% humidity.

Serial-section electron microscopy (ssEM)

At 7 dpf, a larval zebrafish underwent aldehyde specimen fixation followed by heavy metal contrast staining for electron microscopy as described in [72]. The fish was embedded and cured in LX-112 resin, cut in 30nm thick sections using an automated tape collection ultramicrotome (ATUM) system [73] and mounted on silicon wafers (University Wafers, USA) for imaging. The image volume was obtained with a Zeiss multibeam scanning electron microscope (mSEM) equipped with 61 overlapping electron beams [74] following the procedure outlined in [75]. Rigid stitching was performed on raw microscope tiles by extracting SIFT features, with global optimization applied to smooth the results across each section, and elastic stitching used for sections with distortions. Low-resolution thumbnails were generated in real-time, matched with nearby sections, and refined using a spring mesh model to prepare the images for final alignment. We used SOFIMA [76] to obtain a precise alignment of the complete stack, following the procedures outlined previously [75]. Briefly, starting from roughly prealigned sections we computed an optical flow field between each pair of adjacent sections using 8x8 nm^2 EM images. The field vectors were estimated on a regular grid with 40 px spacing. We then modeled each section as an elastic spring mesh grid with edge sizes corresponding to the flow field vector spacing, and with additional 0-length springs representing the flow field vectors. We allowed the system to relax, regularizing the flow field and finding a solution balancing deformation of the original images and cross-sections alignment. We used the final state of the mesh to warp the images into alignment to obtain the 3D stack.

Sections were painted manually using VAST *Lite* version 1.4.1 [77]. 3D objects were exported as mesh files using the ‘vasttools.m’ MATLAB script in VAST

Lite, and processed in Fiji [78], using the 3D viewer plugin [79]. Empty sections in the dataset (marking the position of knife changes) were removed in Blender (blender.org).

Scanning electron microscopy (SEM)

Zebrafish larvae (*ift88*$^{-/-}$ homozygous mutants, lacking cilia) raised in 1× E3 medium were fixed at 4 dpf in 2.5% glutaraldehyde/0.1M sodium cacodylate buffer overnight. Samples were washed in buffer, post-fixed in 2% aqueous osmium tetroxide for 1 hour, and washed in buffer again. Samples were dehydrated through a graded ethanol series (50, 75, 95, 100%), followed by 50:50 hexamethyldisilazane (HMDS):ethanol, and then 100% HMDS. After removal of the HDMS, samples were dried in a fume hood overnight. Samples were mounted onto a pin stub using a Leit-C sticky tab and mounting putty, and gold-coated using an Edwards S150B sputter coater. Samples were imaged in a Tescan Vega3 LMU Scanning Electron Microscope (operating voltage, 15 kV) using a secondary electron detector.

Image processing, quantifications, and statistical analyses

Zeiss LSM 800 confocal images were subjected to Gaussian Blur 3D processing (X:0, Y:0, Z:2) in Fiji. Zeiss LSM 880 Airyscan and LSM 980 Airyscan2 confocal images were subjected to Airyscan processing on Zen Blue 3.7 (Zeiss) using “Auto” Airyscan processing parameters. Further processing (for example, gamma correction, maximum intensity projections, and 3D rendering) was performed in Fiji. For fluorescence intensity quantification, background subtraction was performed with rolling ball radius of 50 pixels, and a ROI was drawn around each cell of interest. Quantification was performed using the Analyze, Measure function in Fiji.

No image quantification was performed in gamma corrected images. Single channel confocal images may be presented with their grayscale values inverted.

Statistical analyses were carried out in GraphPad Prism 10. Datasets were considered normally distributed if they passed the Kolmogorov-Smirnov test. Subsequent statistical tests used are stated in the figure legends. Bars on graphs indicate mean ± standard error of the mean (S.E.M.), unless stated otherwise. *P* values are indicated as follows: $P > 0.05$ (not significant, ns), $P < 0.05$ (*), $P < 0.01$ (**), $P < 0.001$ (***), $P < 0.0001$ (****). Figures were prepared using Adobe Photoshop versions 25.9.0 and 25.11.0 and Adobe Illustrator versions 25.4.1 and 28.6.

Acknowledgements

We are grateful to Cynthia Shiyuan Chen for her help with scRNA-seq data analysis and to Nathalie Jurisch-Yaksi for generous discussion of the adult olfactory transcriptome datasets at early stages of this study. We thank Chris Hill for technical assistance with Scanning Electron Microscopy, which was carried out in the Cryo-Electron Microscopy Facility, University of Sheffield.

Author Contributions

Conceptualization: JP, TP, TTW, SJ; Data Analysis: JP, KYC, TTW; Funding acquisition: FE, JWL, TP, TTW, SJ; Investigation: JP, KYC, TTW, MDP, RS, JBW, YW, SW, MJ, SJ; Methodology: YW, SW, MJ, JWL, FE, VJ ; Resources: TP, TTW, JWL, FE, VJ, MJ, SJ; Supervision: JWL, FE, VJ, SJ, TTW, TP; Validation: JP;

Visualization: JP, NvH, TTW; Writing – original draft: JP, KYC, TTW, SJ; Writing – review and editing: SJ and TTW, with input from MDP, TP and KYC.

Competing Interests

The authors declare no competing interests.

Funding

Work in Kansas City was funded by a NIH (NIDCD) award 1R01DC015488-01A1 to T.P. and by institutional support from the Stowers Institute for Medical Research to T.P. Work in Singapore was funded by a Tier 2 grant (MOE-T2EP30121-0017) from the Ministry of Education, Singapore, to S.J. KYC was funded by an A*STAR Research Attachment Programme Ph.D. studentship (ARAP-2019-01-0014). Work in Sheffield was funded by a Wellcome Trust Investigator Award to T.T.W. (224355/Z/21/Z); imaging in Fig. 3 was performed in the University of Sheffield Wolfson Light Microscopy Facility, using equipment funded by the Medical Research Council (MRC) (MR/X012077/1). F.E. received funding from the National Institutes of Health (U19NS104653 and 1R01NS124017-01), and the Simons Foundation (SCGB 542973 and NC-GB-CULM-00003241-02). The funders had no role in study design, data collection and analysis, decision to publish, or preparation of the manuscript.

Data availability

Raw data underlying this manuscript can be accessed from the Stowers Original Data Repository at http://www.stowers.org/research/publications/libpb-2509.

Figures

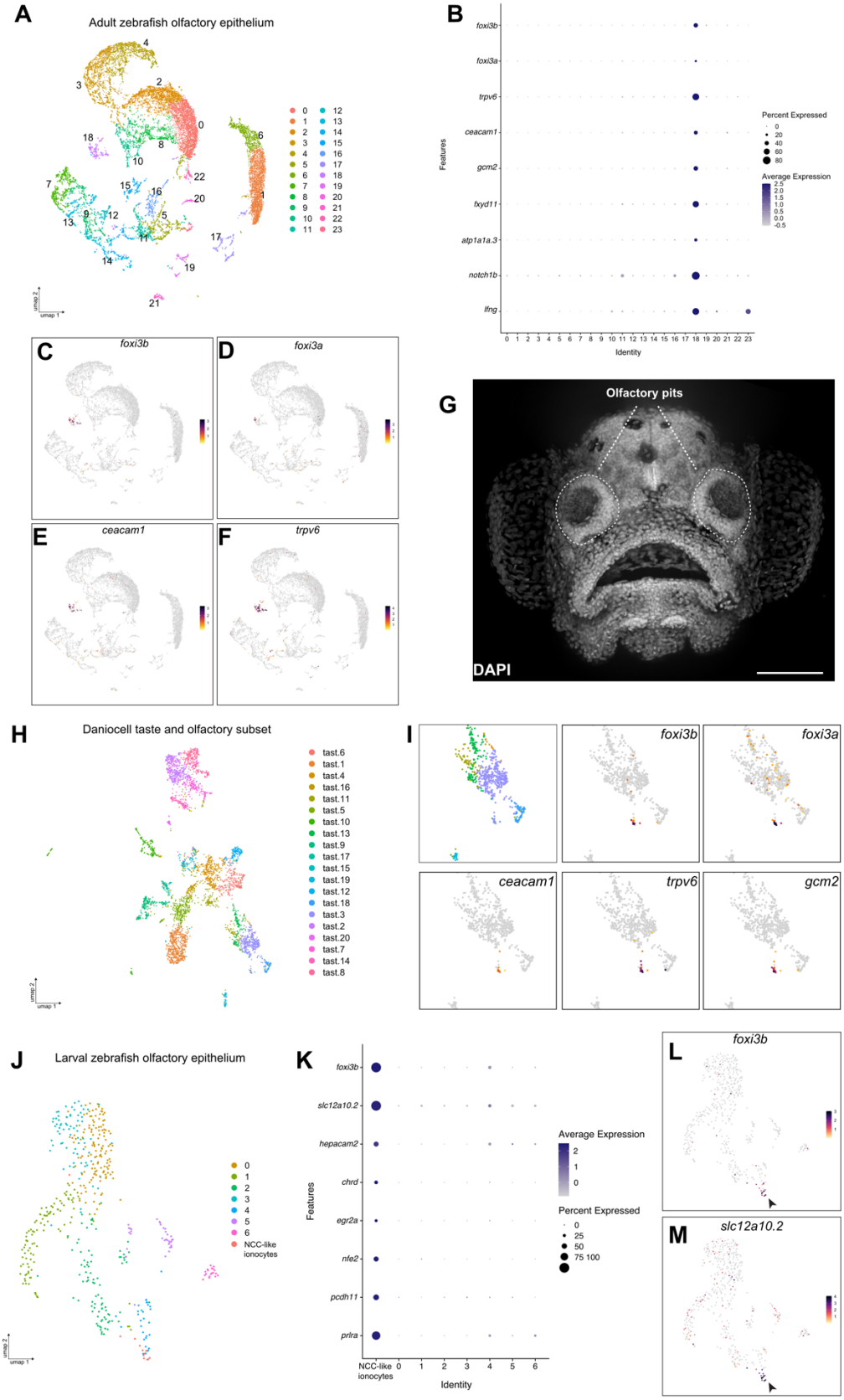

Figure 1. Single-cell RNA sequencing data analysis reveals expression of classical ionocyte-marker genes in the zebrafish olfactory organ

(A) UMAP plot showing 24 unannotated cell clusters (Identity) in the scRNA-seq dataset generated from dissected adult zebrafish olfactory organs. **(B)** Dot plot of data from B depicting several known ionocyte markers expressed in cluster 18. **(C)** Feature plots for *foxi3b*, **(D)** *foxi3a*, **(E)** *ceacam1* and **(F)** *trpv6*. **(G)** Maximum intensity projection of a 4 dpf larva stained with DAPI, frontal view shows the two olfactory pits. Scale bar: 50 µm. **(H)** UMAP plot of taste/olfactory subset from Daniocell [34]. **(I)** Zoomed in feature plots for the ionocyte markers *foxi3b, foxi3a, ceacam1, trpv6* and *gcm2*. **(J)** UMAP plot of olfactory subset from [17]. **(K)** Dot plot of data from J showing several NCC ionocyte markers in *foxi3b*$^{+}$ cells in the olfactory epithelium. **(L)** Feature plots for *foxi3b* and **(M)** *slc12a10.2*.

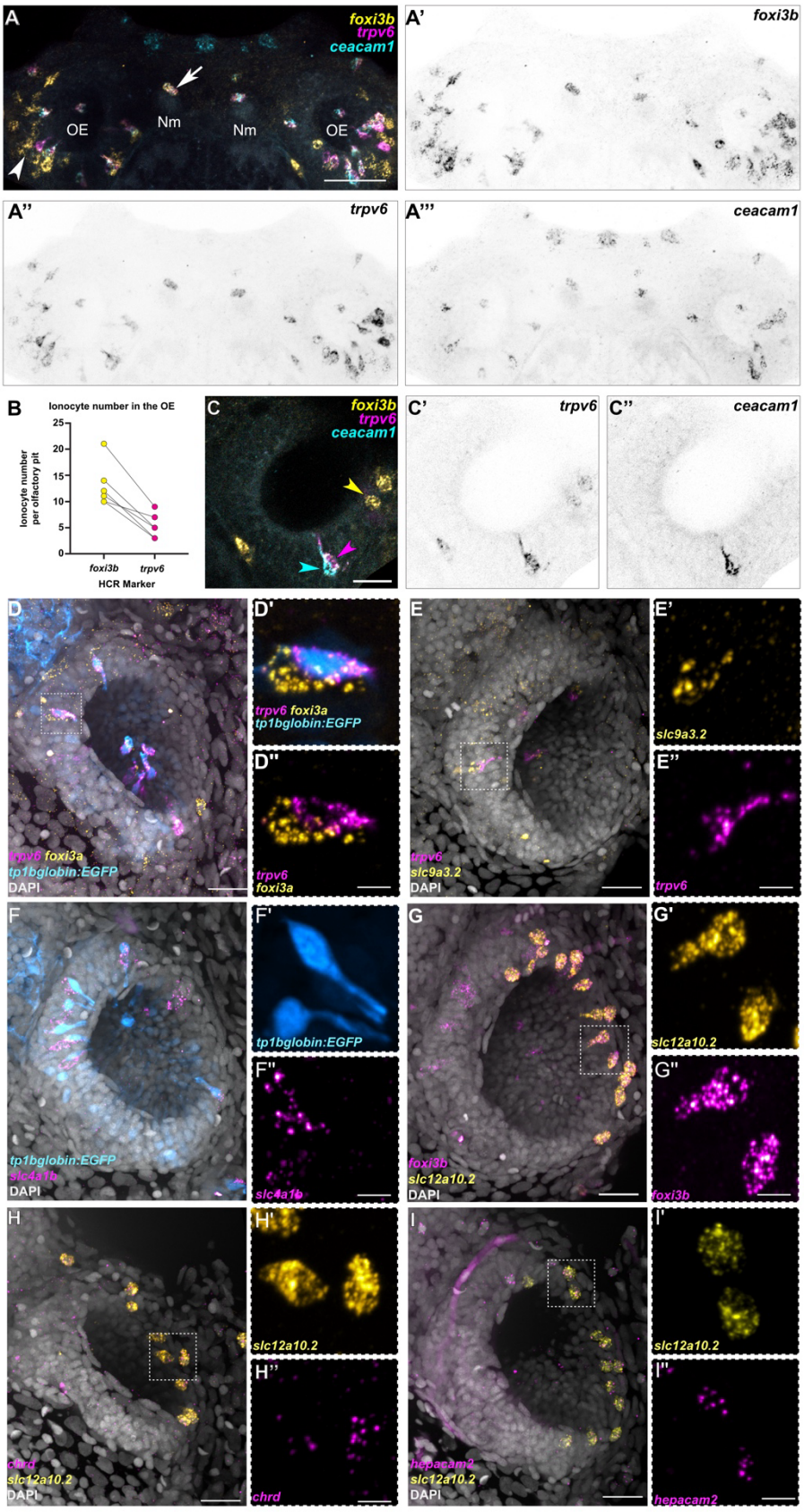

Figure 2. The larval zebrafish olfactory epithelium contains three distinct subtypes of ionocytes

(A–A’’’) Maximum intensity projection of a confocal image of HCR RNA-FISH for *foxi3b* **(A’)**, *trpv6* **(A’’)**, *ceacam1* **(A’’’)**, and merged signals **(A)** in the head of a 5 dpf wild-type larva; dorsal view, anterior to the top. Scale bar: 50 µm. White arrowhead marks an example of an olfactory ionocyte in the posterior-lateral region of the olfactory pit with expression of *foxi3b*. White arrow marks an example neuromast ionocyte with expression of all three selected genes. Abbreviations: OE; olfactory epithelium, Nm; neuromast. **(B)** Numbers of *foxi3b*$^{+}$ ionocytes per olfactory pit in 5 dpf larvae raised in 0.5× E2 medium, of which also express *trpv6*. Connecting lines indicate the same olfactory pit. **(C–C’’)** Confocal image of HCR RNA-FISH signals for *trpv6* **(C’)**, *ceacam1* **(C’’)**, and merged signals **(C)** in the olfactory epithelium of a 5 dpf wild-type larva; dorsal view, anterior to the top, lateral to the right. Scale bar: 20 µm. Magenta and cyan arrowheads mark an example pair of ionocytes, with the magenta arrowhead marking a strong *trpv6* and weak *foxi3b*-expressing cell, and the cyan arrowhead marking a *ceacam1*$^{+}$ cell. Yellow arrowhead marks an example solitary ionocyte, which has strong expression of *foxi3b* and weak expression of *trpv6*. **(D–D’’)** HCR RNA-FISH for *foxi3a* (yellow) and *trpv6* (magenta), combined with the Notch reporter *tp1bglobin:EGFP* (cyan) and DAPI stain (grey). **(E–E’’)** HCR RNA-FISH for *slc9a3.2* (yellow) and *trpv6* (magenta) with DAPI stain (grey). **(F–F’’)** HCR RNA-FISH for *slc4a1b* (magenta) combined with the Notch reporter *tp1bglobin:EGFP* (cyan) and DAPI stain (grey). **(G–G’’)** Maximum intensity projection of a HCR RNA-FISH for *slc12a10.2* (yellow) and *foxi3b* (magenta) with DAPI stain (grey) shows solitary, NCC-like ionocytes in the olfactory epithelium. **(H–H’’)** HCR RNA-FISH for *slc12a10.2* (yellow) and *chrd* (magenta) with DAPI stain (grey). **(I–I’’)** HCR RNA-FISH for *slc12a10.2* (yellow) and *hepacam2* (magenta) with DAPI stain (grey).

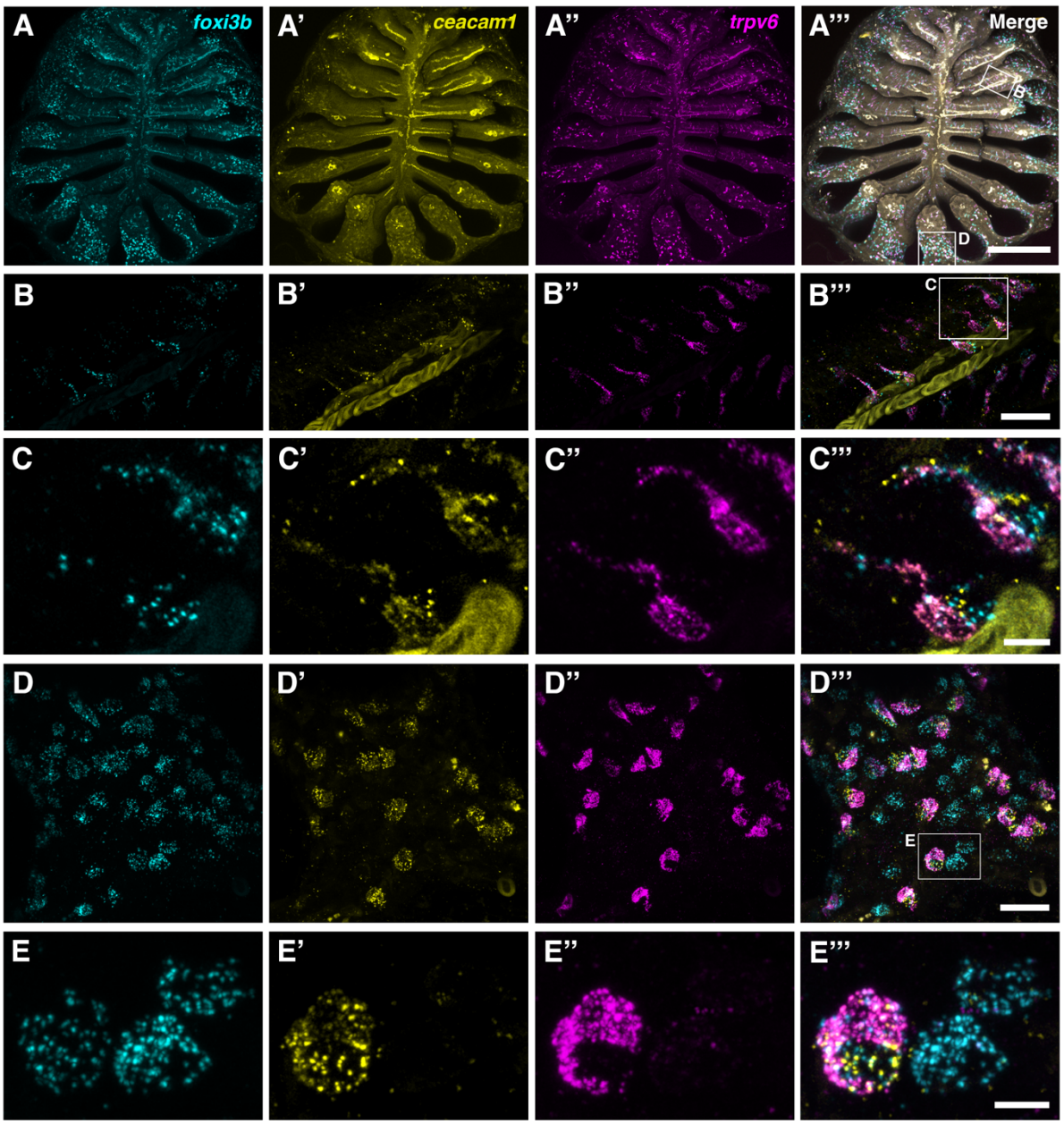

Figure 3. The adult zebrafish olfactory epithelium contains three distinct subtypes of ionocytes

(A–A''') Overview of a dissected adult olfactory rosette. Maximum intensity projections of an Airyscan2 confocal image of HCR RNA-FISH for *foxi3b* **(A)**, *ceacam1* **(A')**, *trpv6* **(A'')**, and merged signals **(A''')**. Scale bar: 200 µm. (**B–B'''**) Enlargement of the boxed region 'B' in A''', within the central (sensory) zone of the olfactory rosette. Maximum intensity projections of selected Airyscan2 confocal

slices; HCR RNA-FISH for *foxi3b* **(B)**, *ceacam1* **(B')**, *trpv6* **(B'')**, and merged signals **(B''')**. Pairs of elongated ionocytes with cell bodies located deep in the epithelium are visible. (The yellow stripe running through the image is autofluorescence from a blood vessel.) Scale bar: 20 μm. (**C–C'''**) Enlargement (maximum intensity projection of selected *z*-slices) of boxed region in B''', featuring two ionocyte pairs: HR-like ionocytes expressing *ceacam1* (yellow) and *foxi3b* (cyan), adjacent to NaR-like ionocytes expressing *trpv6* (magenta) and a low level of *ceacam1*. HCR RNA-FISH for *foxi3b* **(C)**, *ceacam1* **(C')**, *trpv6* **(C'')**, and merged signals **(C''')**. Scale bar: 5 μm. **(D–D''')** Enlargement of boxed region 'D' in A''', within the peripheral (non-sensory, multiciliated) zone of the olfactory rosette. Maximum intensity projections of selected Airyscan2 confocal *z*-slices; HCR RNA-FISH for *foxi3b* **(D)**, *ceacam1* **(D')**, *trpv6* **(D'')**, and merged signals **(D''')**. Both paired and solitary ionocytes are present. Scale bar: 20 μm. **(E–E''').** Enlargement (maximum intensity projection of selected *z*-slices) of the boxed region in D''', featuring one HR-like/NaR-like ionocyte pair, and two NCC-like ionocytes. An HR-like ionocyte, expressing *ceacam1* (yellow) and *foxi3b* (cyan), sits adjacent to an NaR-like ionocyte expressing *trpv6* (magenta) and a lower level of *ceacam1*. The NCC-like ionocytes express *foxi3b* (cyan) but not *ceacam1* or *trpv6*. Ionocytes near the periphery of the rosette were rounded in shape. Scale bar: 5 μm.

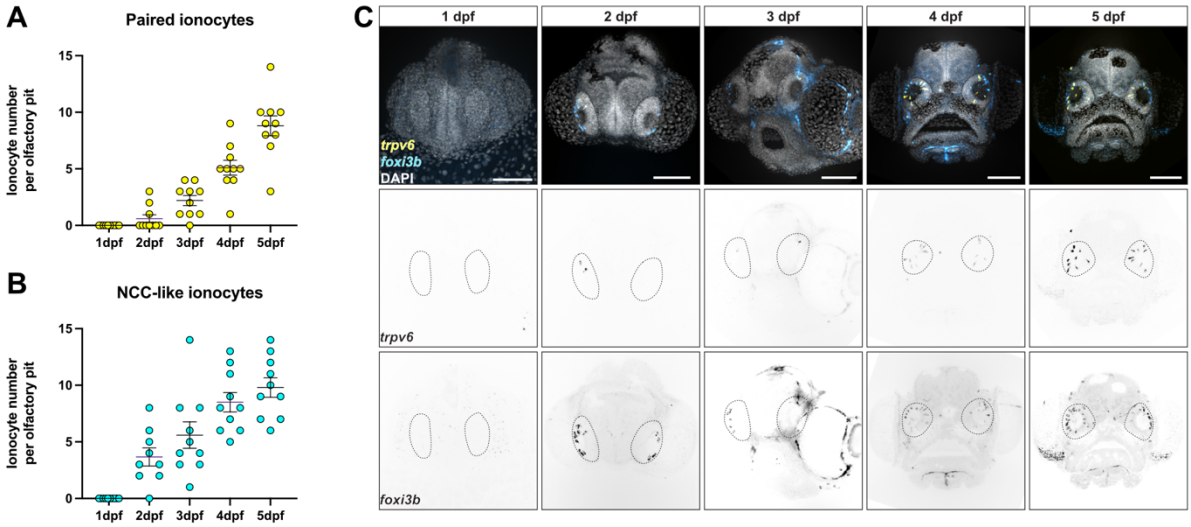

620

621 **Figure 4. The subtypes of olfactory ionocytes develop at different times**

622 **(A)** Developmental time course of NaR-/HR-like ionocyte pairs and **(B)** NCC-like

623 ionocytes from 1 to 5 dpf observed by confocal images of HCR RNA-FISH. **(C)**

624 Representative maximum intensity projection confocal images of HCR RNA-FISH for

625 *trpv6* (yellow) and *foxi3b* (cyan) with DAPI stain (grey) from A and B.

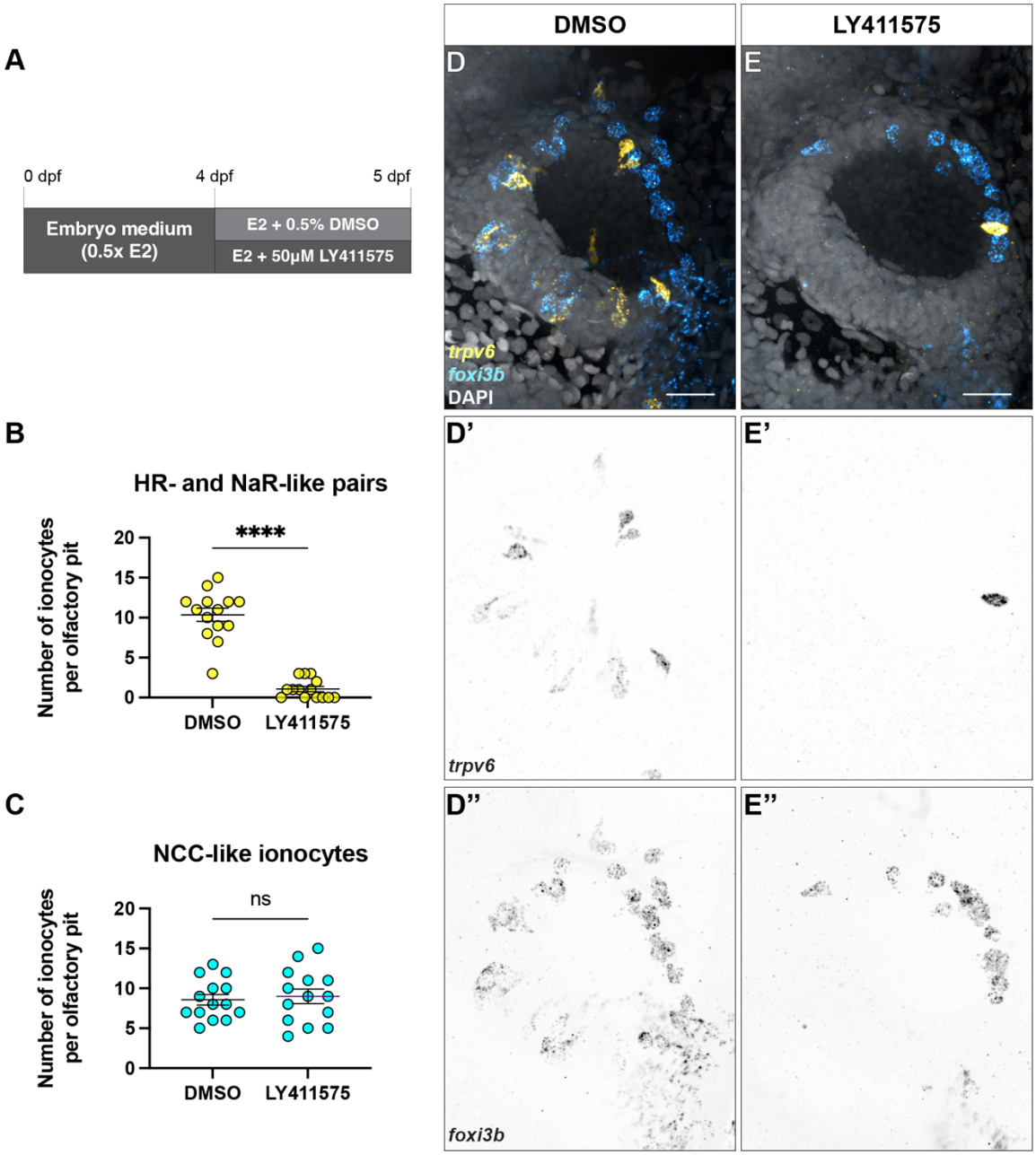

Figure 5. Notch signalling is required for paired ionocyte survival, but does not affect NCC-like ionocyte number

(A) Schematic of experimental design. **(B)** Number of NaR- and HR-like ionocyte pairs in DMSO controls and treated with the Notch inhibitor LY411575. Mann Whitney test ($P < 0.0001$). **(C)** Number of NCC-like ionocytes in DMSO controls and treated with the Notch inhibitor LY411575. Unpaired *t*-test ($P = 0.7070$). **(D–D'')** Representative maximum intensity projection confocal images of HCR RNA-FISH for

634 *trpv6* (yellow) and *foxi3b* (cyan) with DAPI stain (grey) in DMSO-treated and **(E–E'')**

635 LY411575-treated olfactory pits. *N* = 14 olfactory pits per condition. Scale bars: 20

636 µm.

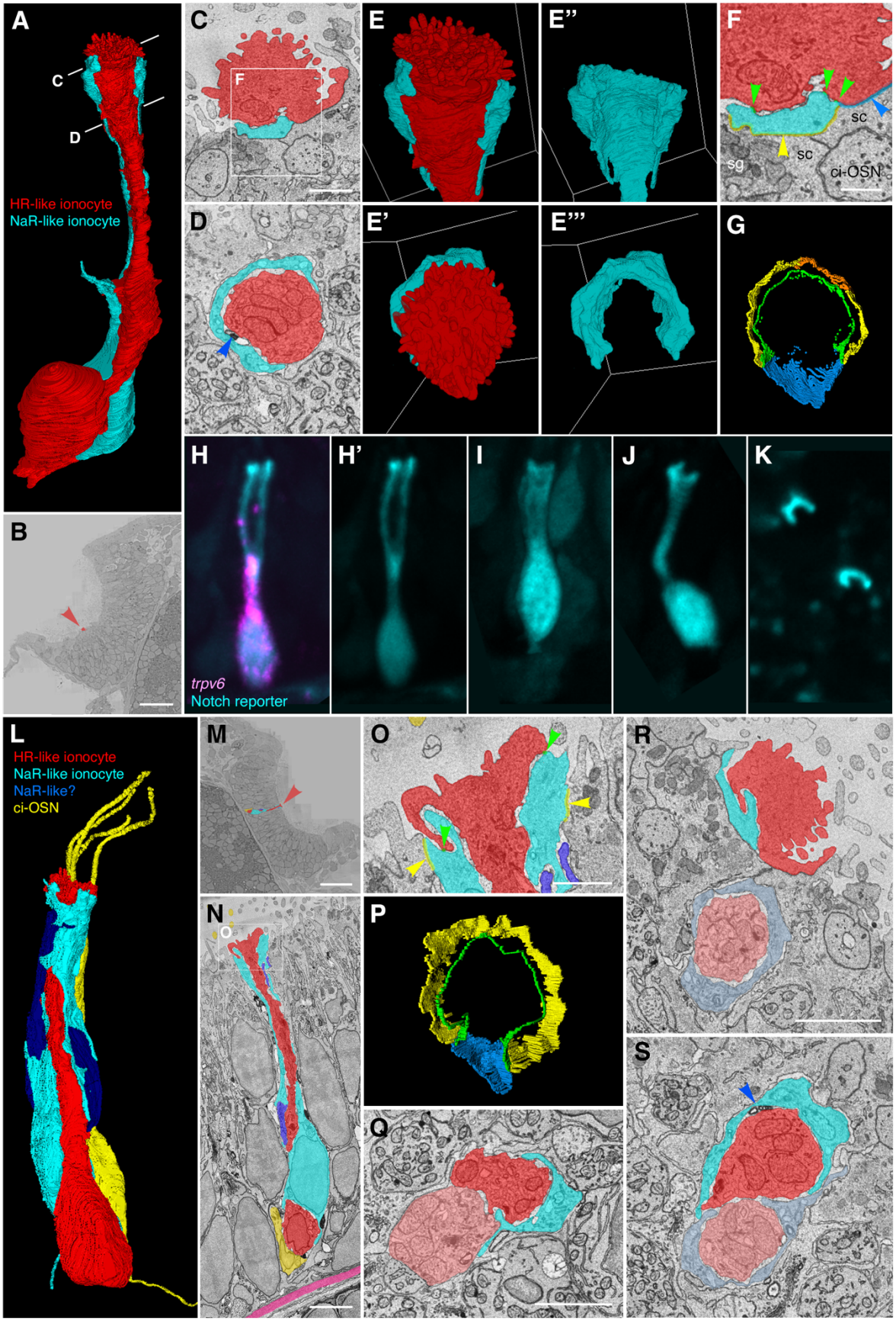

637

Figure 6. Ultrastructure and 3D reconstruction of olfactory HR-like/NaR-like ionocyte cell pairs and multicellular complexes in the wild-type zebrafish larva

(A–G) Representative example of an ionocyte cell pair in the 7 dpf zebrafish larval olfactory pit. The HR-like ionocyte is shown in red, with the NaR-like ionocyte in cyan. **(A)** Volume-EM 3D reconstruction of the cell pair; see also Supplementary Movie 6. **(B)** Location of the cell pair (red arrowhead) in the left olfactory pit (just within the OSN zone). Coronal section; anterior to the top. **(C,D)** Sections at the approximate levels shown in A. Blue arrowhead marks an electron-dense structure in the extracellular space between the cell pair (see also S). **(E–E''')** 3D reconstructions of the apical part of the cell pair, showing the microvillous apical knob of the HR-like ionocyte (red), which projects above the surrounding olfactory supporting cells. The neck of the HR-like ionocyte is wrapped by a thin layer of cytoplasm of the NaR-like cell (cyan). **(F,G)** Tight junctions (zonulae occludentes) of the ionocyte pair. **(F)** Enlargement of the box in C, showing colour-coded labelling of the junctions. Green, shallow tight junction between the two ionocytes; yellow, deep tight junction between NaR-like ionocyte and olfactory supporting cell; orange, deep tight junction between NaR-like ionocyte and multiciliated cell; blue, deep tight junction between HR-like ionocyte and olfactory supporting cell. **Abbreviations:** ci-OSN, ciliated olfactory sensory neuron; sc, olfactory supporting cell; sg, secretory granule. **(G)** 3D reconstruction of the tight junctions (top-down view); see also Supplementary Movie 7.

(H–K) Examples of NaR-like olfactory ionocytes in a live 5 dpf embryo, labelled by EGFP (cyan) in the Notch reporter line *Tg(tp1bglob:EGFP)*. **(H)** Co-expression of EGFP (Notch reporter; cyan) with HCR RNA-FISH for *trpv6* (magenta), confirming the cell as an NaR-like ionocyte (see also Fig. 2E–E"). **(H',I–K)** EGFP (cyan) channel

only. **(I,J)** Additional examples in longitudinal view. **(K)** The apices of EGFP+ cells (NaR-like ionocytes) appear as crescents in a top-down view.

(L–S) Examples of three- and four-cell ionocyte complexes in the wild-type zebrafish olfactory epithelium at 7 dpf. **(L–P)** Example of a 3-cell complex, consisting of an HR-like ionocyte (red), NaR-like ionocyte (cyan), and possible second NaR-like ionocyte (dark blue). A nearby ciliated OSN (yellow) is included for context. **(L)** 3D reconstruction of the ionocyte complex and ciliated OSN; see also Supplementary Movie 8. **(M)** Location of the cells in the OSN zone of the right-hand olfactory pit (red arrowhead). Coronal section. **(N)** Longitudinal section through the complex, showing close association between the HR-like ionocyte (red) and the ciliated OSN (yellow) at the base, and location relative to the basal lamina (pink). **(O)** Enlargement of the box in C, showing colour-coded labelling of the tight junctions of the HR-like (red) and NaR-like (cyan) cells (colour code as in F). **(P)** 3D reconstruction of the tight junctions of the HR-like (red) and NaR-like (cyan) cells (top-down view; compare to G; see also Supplementary Movie 9). **(Q)** Example section through a three-cell complex consisting of an HR-like cell (red), an NaR-like cell (cyan), and possible second HR-like cell (pink). **(R,S)** Example sections through a four-cell complex consisting of two HR-like/NaR-like pairs. The cell pairs are separate at their apices (R), but are closely associated beneath the epithelial surface (S). Blue arrowhead in S marks electron-dense structures between the ionocytes.

Scale bars: B, 20 μm; **C**; 1 μm (applies to **D–E’’’**, **G**); **F**, 0.5 μm; **M**, 20 μm; **N**, 3 μm; **O**, 1 μm (applies to **P**); **Q**, 2 μm; **R**, 2 μm (applies to **S**).

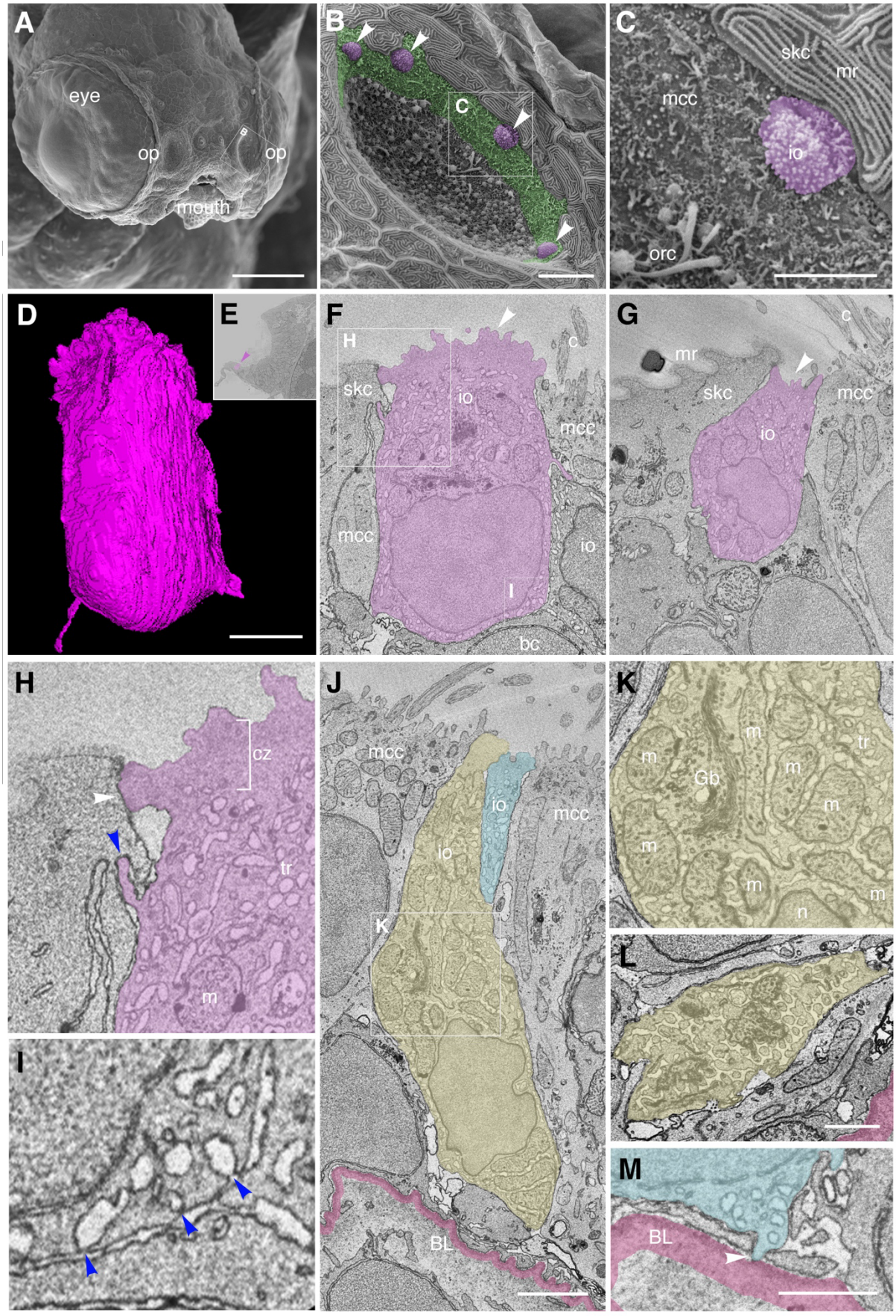

685

Figure 7. Ultrastructure and 3D reconstruction of NCC-like olfactory ionocytes in the non-sensory multiciliated cell zone of the zebrafish olfactory pit

(A–C) Scanning electron micrographs of an *ift88*$^{-/-}$ zebrafish mutant embryo at 4 dpf. **(A)** Whole head showing location of the two olfactory pits (op). **(B)** Enlargement of the left-hand olfactory pit, boxed in A. The rounded apical surfaces of four ionocytes (presumed NCC-like) are highlighted in magenta (arrowheads). The peripheral zone of non-sensory multiciliated cells (mcc) is highlighted in green. (All olfactory cilia are missing in the *ift88*$^{-/-}$ mutant, allowing visualization of the apical surface of cells in the pit.) **(C)** Enlargement of the boxed region in **B**. An ionocyte (magenta) sits in the MCC zone, in contact with a skin cell with microridges (top right). The rods of two or three olfactory rod cells are also visible (bottom left; see also Fig. 3I in [80]) .

(D–M) Ultrastructure and 3D reconstruction of ionocytes in the non-sensory multiciliated zone of the olfactory pit in a wild-type zebrafish larva at 7 dpf. **(D)** 3D reconstruction of a presumed NCC-like ionocyte, showing the microvillous apical surface. **(E)** Location of the ionocyte in D (magenta; arrowhead) at the lateral edge of the left olfactory pit. Coronal section. **(F,G)** Selected sections through the ionocyte shown in D, highlighted in magenta. The ionocyte makes contact with at least four other cell types: apically, with a skin cell on one side and a multiciliated cell on the other; basolaterally, with multiciliated cells, a basal cell, and another ionocyte. The microvillous apical surface is rounded in one area (F, arrowhead) but also forms a pit-like structure (G, arrowhead) in the same cell. **(H)** Enlargement of the boxed region in F (top left), highlighting tight junctional contact (white arrowhead) and interdigitation (blue arrowhead) between the ionocyte and a neighbouring skin cell. **(I)** Enlargement of the boxed region in F (bottom right), showing that pores where the tubular reticulum meets the plasma membrane are covered by a thin electron-dense

structure (blue arrowheads). **(J)** Two examples of more elongated ionocytes highlighted in yellow and blue, with their apices sitting between multiciliated cells. **(K)** Enlargement of the boxed region in J, showing mitochondria-rich cytoplasm, Golgi apparatus and extensive tubular reticulum. **(L)** Section through the base of the yellow cell in J, showing the tubular reticulum. **(M)** An end-foot (arrowhead) of the blue ionocyte in J makes direct contact with the basal lamina (pink).

Abbreviations: bc, basal cell; BL, basal lamina (pink); c, cilia of multiciliated cell; cz, cortical zone (free of mitochondria; bracketed in H); Gb, Golgi body; io, presumed NCC-like ionocyte; m, mitochondrion; mcc, multiciliated cell; mr, microridges on skin cell; n, cell nucleus; op, olfactory pit; orc, olfactory rod cell (apical rods visible); skc, skin cell; tr, tubular reticulum.

Scale bars: A, 100 µm; **B**, 10 µm; **C**, 5 µm; **D**, 2 µm (applies to **F, G**); **J**; 2 µm; **L**, 1 µm; **M**, 1 µm.

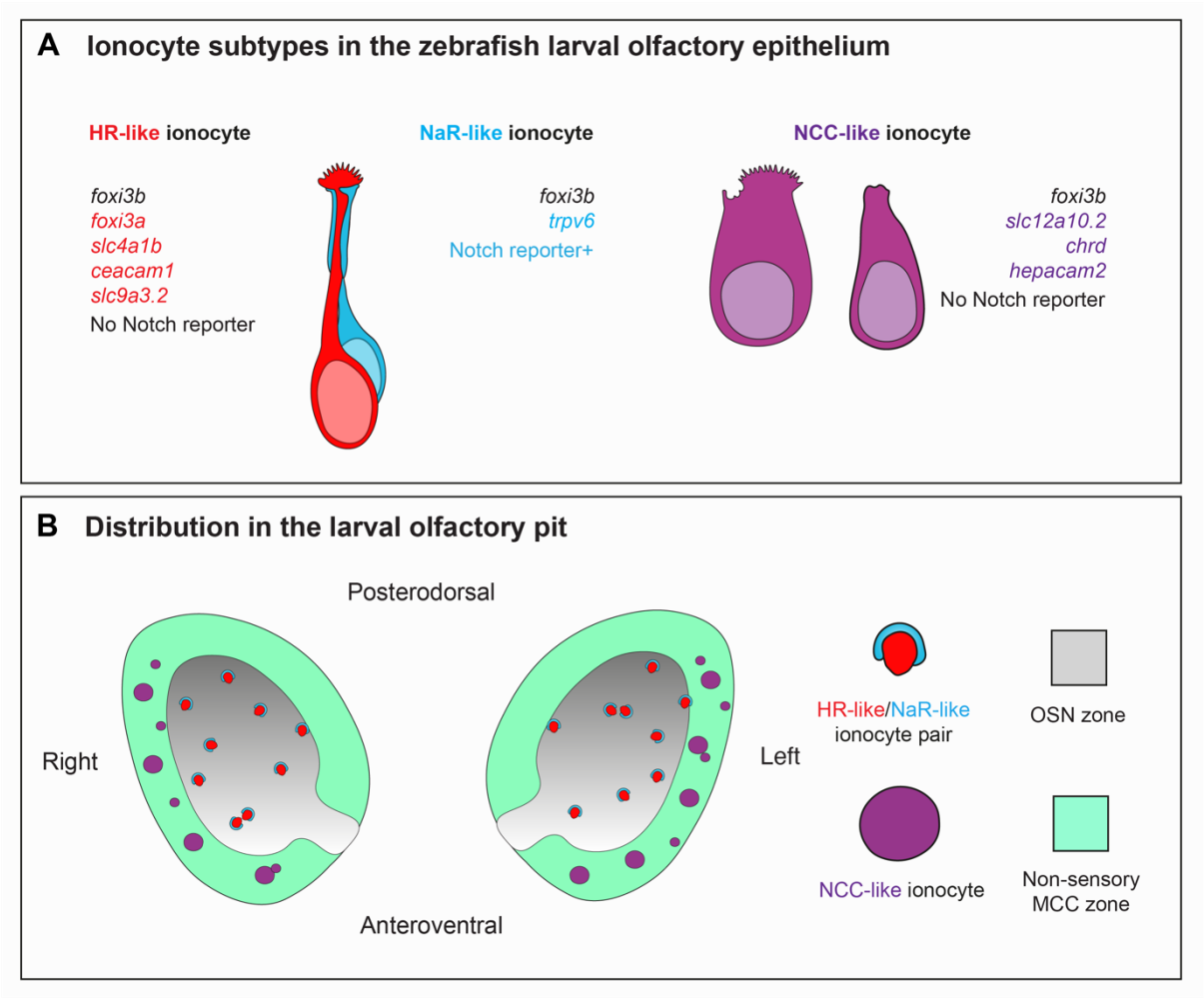

Figure 8. Ionocytes in the zebrafish larval olfactory epithelium

(A) Schematic of HR- and NaR-like ionocyte pairs and NCC-like ionocytes in the zebrafish larval olfactory epithelium and their gene expression characterised in this study. The NCC-like cells have variable morphologies, some with a rounded microvillous apical surface. **(B)** Schematic showing distribution of ionocytes in the zebrafish larval olfactory pit (viewed from the front; not to scale). Abbreviations: MCC, multiciliated cell; OSN, olfactory sensory neuron.

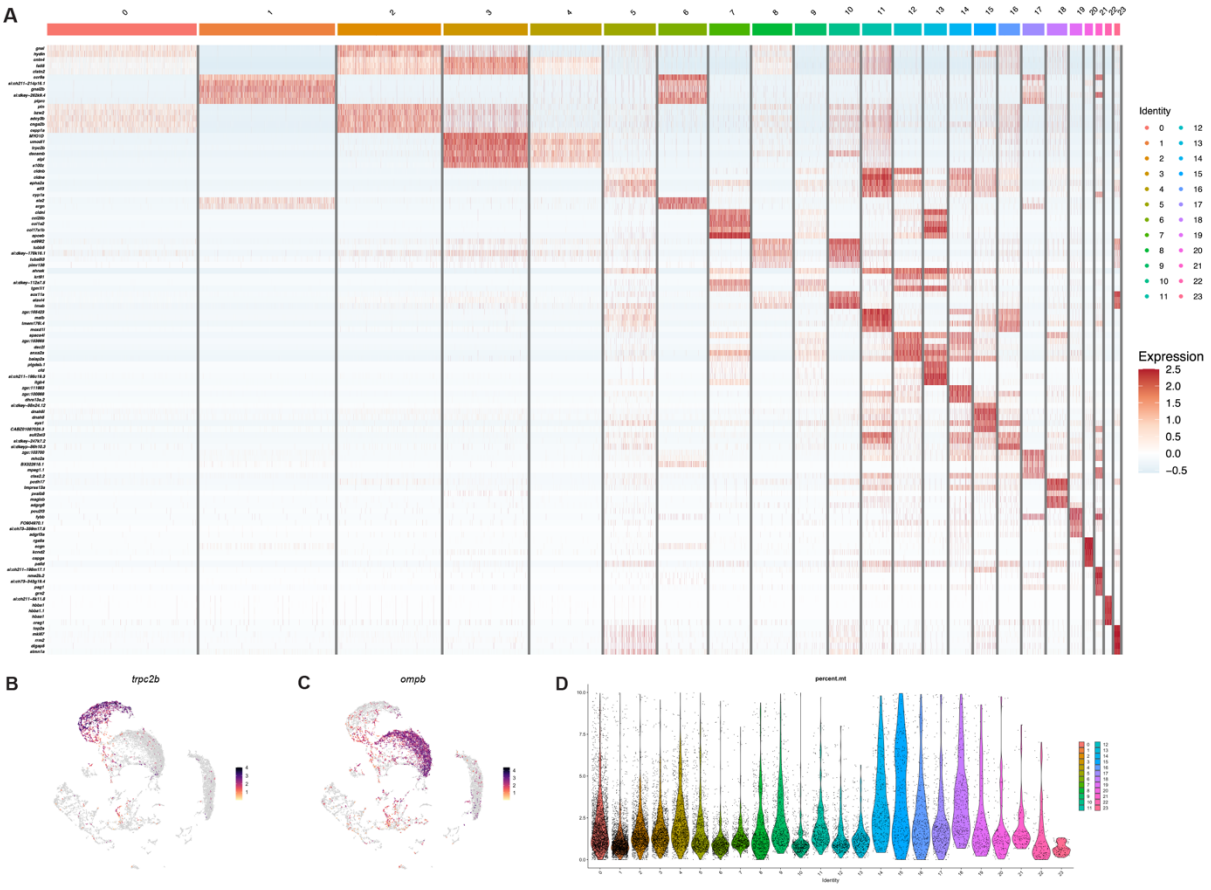

Figure S1, related to Figure 1

(A) Heatmap showing top 5 highest expressing genes based on LogFC on the clusters obtained in the dataset from dissected adult zebrafish olfactory organs. **(B)** Feature plots of *trpc2b* and **(C)** *ompb.* **(D)** Violin plot showing the percentage of mitochondrial genes in the dataset.

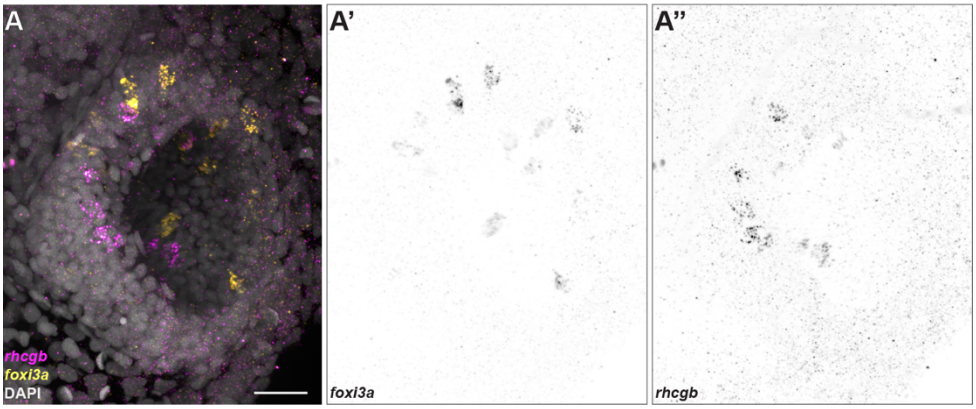

Figure S2, related to Figure 2

(A) Maximum intensity projection of a confocal image showing HCR RNA-FISH signals for *foxi3a* (yellow) and *rhcgb* (magenta) with DAPI stain (grey). **(A')** Individual channels for *foxi3a* and **(A'')** *rhcgb*. Scale bar: 20 µm.

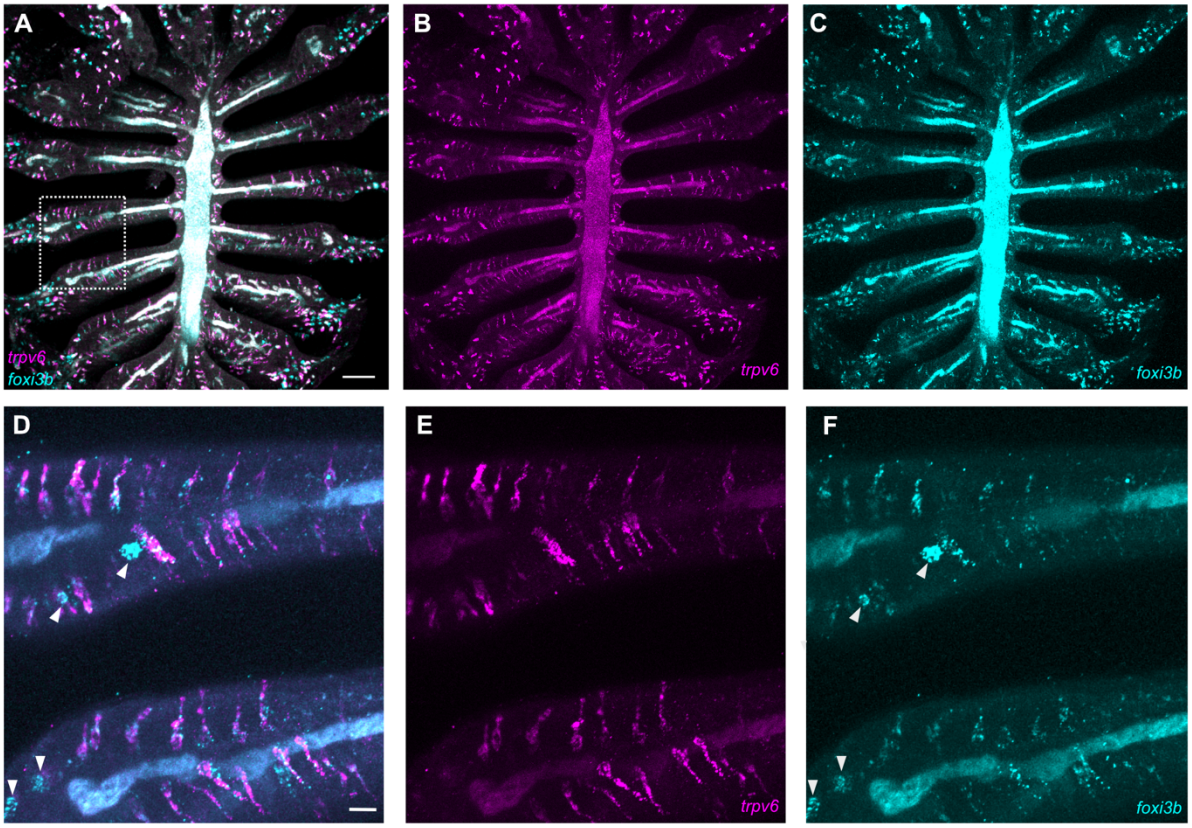

Figure S3, related to Figure 3

(A-C) Overview of an adult olfactory rosette, showing expression of *trpv6* **(B)** and *foxi3b* **(C)**. **(D-F)** High magnification view of the region outlined in panel A. The arrowheads indicate solitary NCC-like ionocytes, which express *foxi3b* and have a rounded shape. These are distinct from elongated pairs of cells that express either *foxi3b* or *trpv6*. Scale bar: 50 μm in panel A, 20 μm in panel D.

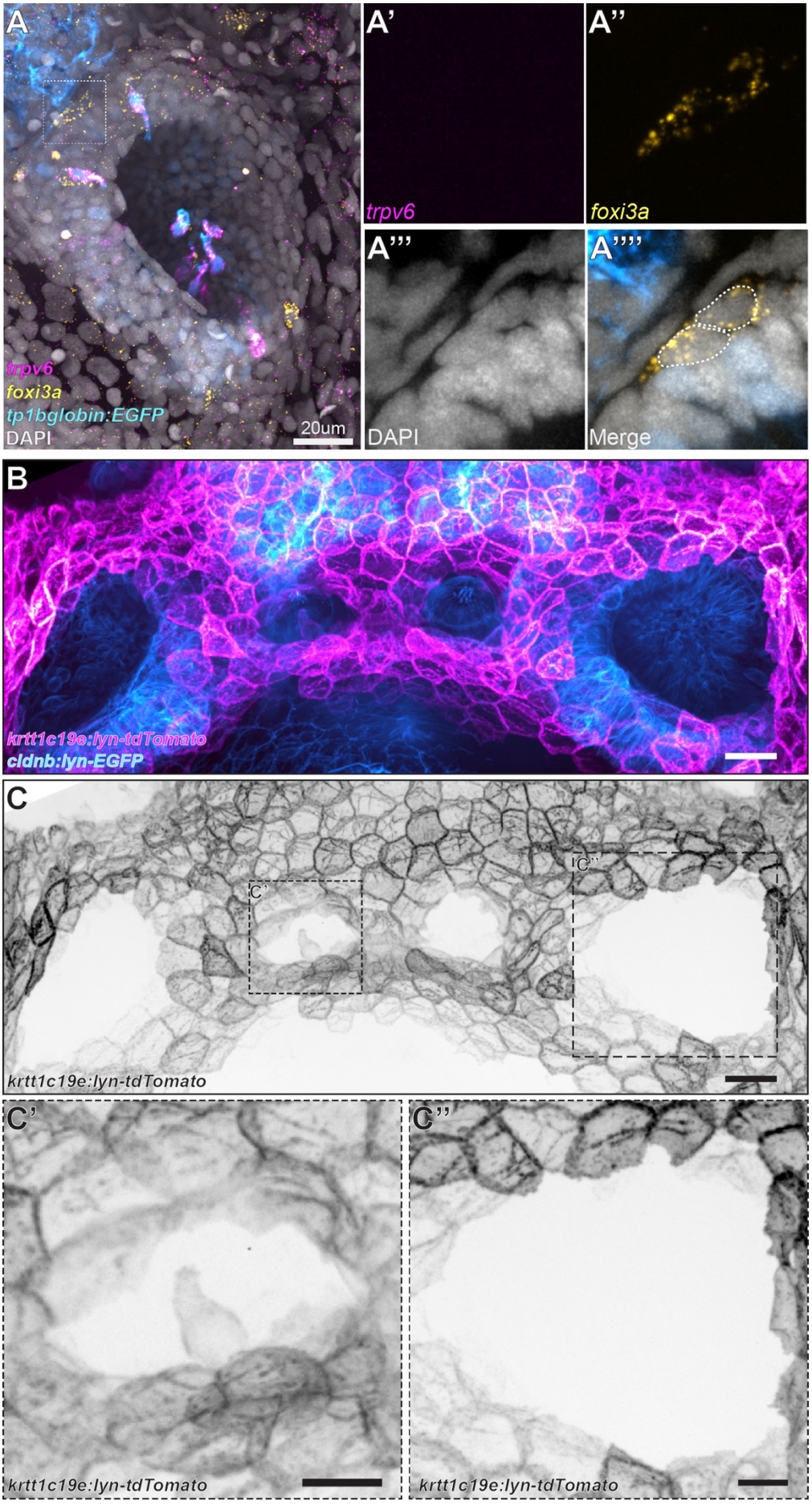

757

Figure S4, related to Figure 4

(A–A’’’’) *foxi3a*+ cells (yellow) at the edge of an olfactory pit, as shown by HCR RNA-FISH. **(B)** Maximum intensity projection of a confocal image from *Tg(-8.0cldnb:lyn-EGFP)^{zf106Tg};Tg(krtt1c19e:lyn-tdTomato)^{sq16}* transgenic larva shows a pair of Nm ionocytes in the neuromast, but no tdTomato^{+} cells in the olfactory pit. **(C)** Single channel image of *krtt1c19e:lyn-tdTomato*. **(C’)** Enlargement of a neuromast containing tdTomato^{+} Nm ionocytes. **(C’’)** Enlargement of an olfactory pit containing no tdTomato^{+} cells.

Supplementary Material

Supplementary Table 1. Differentially expressed genes in dissected adult zebrafish olfactory organ scRNA-seq dataset. This spreadsheet contains the differentially expressed gene list (cluster markers) of olfactory cell types from the integrated adult dataset via Seurat::FindAllMarkers function with default parameters. Ionocytes are on cluster 18.

Supplementary Table 2. Differentially expressed genes in larval 5 dpf olfactory cell subset. This spreadsheet contains the differentially expressed gene list (cluster markers) of olfactory cell types from the subsetted larval dataset via Seurat::FindAllMarkers function with default parameters.

Movie 1. 3D rendering of an embryonic olfactory pit depicting HR- and NaR-like ionocytes. HCR RNA-FISH for *trpv6* (magenta) and *foxi3a* (yellow), combined with the Notch reporter *tp1bglobin:EGFP* (cyan), shows spatial distribution of ionocyte pairs in the larval 5 dpf olfactory pit. Initial image is a frontal view of the left olfactory pit, with dorsal to the top and lateral to the right.

Movie 2. 3D rendering of an embryonic olfactory pit showing NCC-like ionocytes. HCR RNA-FISH for *slc12a10.2* (yellow) and *foxi3b* (magenta), combined with the Notch reporter *tp1bglobin:EGFP* (cyan), showing the spatial distribution of ionocyte pairs in the larval 5 dpf olfactory pit. Initial image is a frontal view of the left olfactory pit, with dorsal to the top and lateral to the right.

Movie 3. New olfactory ionocytes do not express skin transgenes. Time lapse from *Tg(-8.0cldnb:lyn-EGFP)*^{zf106Tg}*;Tg(krtt1c19e:lyn-tdTomato)*^{sq16} transgenic

788 zebrafish larva showing pairs of tdTomato^{+} Nm ionocytes (arrow, middle panel)
789 invading neuromasts, but no positive cells in the olfactory epithelium.

790 **Movie 4. Differentiation of ionocyte pairs in a larval olfactory pit and**
791 **neuromast.** Time lapse from a 3 dpf transgenic zebrafishlarva (*Tg(dld:hist2h2l-*
792 *EGFP)^{psi84}*) showing a pair of ionocytes (cyan and yellow dots; visible at the start of
793 the recording) invading the neuromast. At ~90 hours ionocytes are visible in the
794 olfactory pit (red and cyan dots). No invasion was detected.

795 **Movie 5. Ionocyte pair development in a larval olfactory pit.** Time lapse from a 3
796 dpf transgenic zebrafish larva (*Tg(dld:hist2h2l-EGFP)^{psi84}*) showing the appearance
797 of a pair of olfactory ionocytes (red and cyan dots). The pair is visible at
798 approximately 85 hours, and move around together.

799 **Movie 6. 3D reconstruction of an HR-like/NaR-like ionocyte pair from a 7 dpf**
800 **wild-type olfactory pit.** 360° rotation of Fig. 6A. Red, HR-like cell; cyan, NaR-like
801 cell.

802 **Movie 7. 3D reconstruction of the tight junctions of an HR-like/NaR-like**
803 **ionocyte pair.** 360° rotation of Fig. 6G; compare to Movie 9. Green, shallow tight
804 junction between the two ionocytes; yellow, deep tight junction between NaR-like
805 ionocyte and olfactory supporting cell; orange, deep tight junction between NaR-like
806 ionocyte and multiciliated cell; blue, deep tight junction between HR-like ionocyte
807 and olfactory supporting cell.

808 **Movie 8. 3D reconstruction of a 3-cell ionocyte complex from a 7 dpf wild-type**
809 **olfactory pit.** 360° rotation of Fig. 6L. Red, HR-like cell; cyan, NaR-like cell; dark

blue, possible second NaR-like cell; yellow, ciliated OSN (not part of the ionocyte complex, but included for context and scale).

Movie 9. 3D reconstruction of the tight junctions between the HR-like (red) and NaR-like (cyan) ionocytes in Fig. 6L. 360° rotation of Fig. 6P; compare to Movie 7. Green, shallow tight junction between the two ionocytes; yellow, deep tight junction between NaR-like ionocyte (cyan) and olfactory supporting cell; blue, deep tight junction between HR-like ionocyte (red) and olfactory supporting cell.

References

1. Kleene SJ. Origin of the chloride current in olfactory transduction. Neuron. 1993;11: 123–132. doi:10.1016/0896-6273(93)90276-w

2. Reuter D, Zierold K, Schröder WH, Frings S. A depolarizing chloride current contributes to chemoelectrical transduction in olfactory sensory neurons in situ. J Neurosci : Off J Soc Neurosci. 1998;18: 6623–30.

3. Kaneko H, Putzier I, Frings S, Kaupp UB, Gensch T. Chloride accumulation in mammalian olfactory sensory neurons. The Journal of neuroscience : the official journal of the Society for Neuroscience. 2004;24: 7931–7938. doi:10.1523/jneurosci.2115-04.2004

4. Reisert J, Reingruber J. Ca2+-activated Cl− current ensures robust and reliable signal amplification in vertebrate olfactory receptor neurons. Proc Natl Acad Sci. 2019;116: 1053–1058. doi:10.1073/pnas.1816371116

5. Selvaraj S, Liu K, Robinson AM, Epstein VA, Conley DB, Kern RC, et al. In Vivo Determination of Mouse Olfactory Mucus Cation Concentrations in Normal and Inflammatory States. PLoS ONE. 2012;7: e39600. doi:10.1371/journal.pone.0039600

6. Spence R, Fatema MK, Reichard M, Huq KA, Wahab MA, Ahmed ZF, et al. The distribution and habitat preferences of the zebrafish in Bangladesh. J Fish Biol. 2006;69: 1435–1448. doi:10.1111/j.1095-8649.2006.01206.x

7. Friedrich RW, Habermann CJ, Laurent G. Multiplexing using synchrony in the zebrafish olfactory bulb. Nat Neurosci. 2004;7: 862–871. doi:10.1038/nn1292

8. Niessing J, Friedrich RW. Olfactory pattern classification by discrete neuronal network states. Nature. 2010;465: 47–52. doi:10.1038/nature08961

9. Hansen A, Zeiske E. Development of the olfactory organ in the zebrafish, Brachydanio rerio. J Comp Neurol. 1993;333: 289–300. doi:10.1002/cne.903330213

842 10. Hansen A, Zeiske E. The peripheral olfactory organ of the zebrafish, Danio rerio:
843 an ultrastructural study. Chemical Senses. 1998;23: 39–48. Available:
844 http://eutils.ncbi.nlm.nih.gov/entrez/eutils/elink.fcgi?dbfrom=pubmed&id=9530968&re
845 tmode=ref&cmd=prlinks
846 11. Saraiva LR, Ahuja G, Ivandic I, Syed AS, Marioni JC, Korsching SI, et al.
847 Molecular and neuronal homology between the olfactory systems of zebrafish and
848 mouse. Scientific reports. 2015;5: 11487. doi:10.1038/srep11487
849 12. Hwang P-P, Chou M-Y. Zebrafish as an animal model to study ion homeostasis.
850 Pflügers Arch - Eur J Physiol. 2013;465: 1233–1247. doi:10.1007/s00424-013-1269-
851 1
852 13. Guh Y-J, Lin C-H, Hwang P-P. Osmoregulation in zebrafish: ion transport
853 mechanisms and functional regulation. EXCLI J. 2015;14: 627–659.
854 doi:10.17179/excli2015-246
855 14. Casellas CP, Pleguezuelos-Manzano C, Rookmaaker MB, Verhaar MC, Clevers
856 H. Transcriptomic profile comparison reveals conservation of ionocytes across
857 multiple organs. Sci Rep. 2023;13: 3516. doi:10.1038/s41598-023-30603-1
858 15. Ualiyeva S, Lemire E, Wong C, Perniss A, Boyd AA, Avilés EC, et al. A nasal
859 cell atlas reveals heterogeneity of tuft cells and their role in directing olfactory stem
860 cell proliferation. Sci Immunol. 2024;9: eabq4341. doi:10.1126/sciimmunol.abq4341
861 16. Honda K, Kim SH, Kelly MC, Burns JC, Constance L, Li X, et al. Molecular
862 architecture underlying fluid absorption by the developing inner ear. eLife. 2017;6:
863 e26851. doi:10.7554/elife.26851
864 17. Peloggia J, Münch D, Meneses-Giles P, Romero-Carvajal A, Lush ME, Lawson
865 ND, et al. Adaptive cell invasion maintains lateral line organ homeostasis in
866 response to environmental changes. Dev Cell. 2021;56: 1296-1312.e7.

867 doi:10.1016/j.devcel.2021.03.027

868 18. Hwang P. Ultrastructural study on multicellular complex of chloride cells in

869 teleosts. Bull Inst Zool, Academia Sinica. 1988.

870 19. Cozzi RRF, Robertson GN, Spieker M, Claus LN, Zaparilla GMM, Garrow KL, et

871 al. Paracellular pathway remodeling enhances sodium secretion by teleost fish in

872 hypersaline environments. J Exp Biol. 2015;218: 1259–1269.

873 doi:10.1242/jeb.117317

874 20. Bertmar G. Labyrinth cells, a new cell type in vertebrate olfactory organs. Z für

875 Zellforsch Mikrosk Anat. 1972;132: 245–256. doi:10.1007/bf00307014

876 21. Ruzhinskaya NN, Gdovskii PA, Devitsina GV. Chloride Cells, A Constituent of

877 the Fish Olfactory Epithelium. J Evol Biochem Physiol. 2001;37: 89–94.

878 doi:10.1023/a:1017526204623

879 22. Ghosh SK. Histoanatomy and surface ultrastructure of the olfactory organ of the

880 freshwater tank goby, Glossogobius giuris (Hamilton, 1822). Fish Aquat Life.

881 2020;28: 141–148. doi:10.2478/aopf-2020-0017

882 23. Hsiao C-D, You M-S, Guh Y-J, Ma M, Jiang Y-J, Hwang P-P. A Positive

883 Regulatory Loop between foxi3a and foxi3b Is Essential for Specification and

884 Differentiation of Zebrafish Epidermal Ionocytes. PLoS ONE. 2007;2: e302.

885 doi:10.1371/journal.pone.0000302

886 24. Jänicke M, Carney TJ, Hammerschmidt M. Foxi3 transcription factors and Notch

887 signaling control the formation of skin ionocytes from epidermal precursors of the

888 zebrafish embryo. Dev Biol. 2007;307: 258–271. doi:10.1016/j.ydbio.2007.04.044

889 25. Hwang P-P. Ion uptake and acid secretion in zebrafish (Danio rerio). J Exp Biol.

890 2009;212: 1745–1752. doi:10.1242/jeb.026054

891 26. Pan T-C, Liao B-K, Huang C-J, Lin L-Y, Hwang P-P. Epithelial Ca2+ channel

892 expression and Ca2+ uptake in developing zebrafish. Am J Physiol-Regul, Integr
893 Comp Physiol. 2005;289: R1202–R1211. doi:10.1152/ajpregu.00816.2004
894 27. Kowalewski J, Paris T, Gonzalez C, Lelièvre E, Valencia LC, Boutrois M, et al.
895 Characterization of a member of the CEACAM protein family as a novel marker of
896 proton pump-rich ionocytes on the zebrafish epidermis. PLoS ONE. 2021;16:
897 e0254533. doi:10.1371/journal.pone.0254533
898 28. Wang Y-F, Tseng Y-C, Yan J-J, Hiroi J, Hwang P-P. Role of SLC12A10.2, a Na-
899 Cl cotransporter-like protein, in a Cl uptake mechanism in zebrafish (Danio rerio).
900 Am J Physiol-Regul, Integr Comp Physiol. 2009;296: R1650–R1660.
901 doi:10.1152/ajpregu.00119.2009
902 29. Shih S-W, Yan J-J, Lu S-W, Chuang Y-T, Lin H-W, Chou M-Y, et al. Molecular
903 Physiological Evidence for the Role of Na+-Cl− Co-Transporter in Branchial Na+
904 Uptake in Freshwater Teleosts. Int J Mol Sci. 2023;24: 6597.
905 doi:10.3390/ijms24076597
906 30. Kraus A, Huertas M, Ellis L, Boudinot P, Levraud J-P, Salinas I. Intranasal
907 delivery of SARS-CoV-2 spike protein is sufficient to cause olfactory damage,
908 inflammation and olfactory dysfunction in zebrafish. Brain, Behav, Immun. 2022;102:
909 341–359. doi:10.1016/j.bbi.2022.03.006
910 31. Saito K, Nakamura N, Ito Y, Hoshijima K, Esaki M, Zhao B, et al. Identification of
911 Zebrafish Fxyd11a Protein that is Highly Expressed in Ion-Transporting Epithelium of
912 the Gill and Skin and its Possible Role in Ion Homeostasis. Front Physiol. 2010;1:
913 129. doi:10.3389/fphys.2010.00129
914 32. Liao B-K, Chen R-D, Hwang P-P. Expression regulation of Na+-K+-ATPase α1-
915 subunit subtypes in zebrafish gill ionocytes. Am J Physiol-Regul, Integr Comp
916 Physiol. 2009;296: R1897–R1906. doi:10.1152/ajpregu.00029.2009

917 33. Peloggia J, Lush ME, Tsai Y-Y, Wood C, Piotrowski T. Environmental and
918 molecular control of tissue-specific ionocyte differentiation in zebrafish. bioRxiv.
919 2024; 2024.01.12.575421. doi:10.1101/2024.01.12.575421
920 34. Sur A, Wang Y, Capar P, Margolin G, Prochaska MK, Farrell JA. Single-cell
921 analysis of shared signatures and transcriptional diversity during zebrafish
922 development. Dev Cell. 2023;58: 3028-3047.e12. doi:10.1016/j.devcel.2023.11.001
923 35. Farrell JA, Wang Y, Riesenfeld SJ, Shekhar K, Regev A, Schier AF. Single-cell
924 reconstruction of developmental trajectories during zebrafish embryogenesis.
925 Science. 2018;360. doi:10.1126/science.aar3131
926 36. Trivedi V, Choi HMT, Fraser SE, Pierce NA. Multidimensional quantitative
927 analysis of mRNA expression within intact vertebrate embryos. Development.
928 2018;145: dev156869. doi:10.1242/dev.156869
929 37. Nakada T, Hoshijima K, Esaki M, Nagayoshi S, Kawakami K, Hirose S.
930 Localization of ammonia transporter Rhcg1 in mitochondrion-rich cells of yolk sac,
931 gill, and kidney of zebrafish and its ionic strength-dependent expression. Am J
932 Physiol-Regul, Integr Comp Physiol. 2007;293: R1743–R1753.
933 doi:10.1152/ajpregu.00248.2007
934 38. Fridman S. Ontogeny of the Osmoregulatory Capacity of Teleosts and the Role
935 of Ionocytes. Front Mar Sci. 2020;7: 709. doi:10.3389/fmars.2020.00709
936 39. Laurent P, Chevalier C, Wood CM. Appearance of cuboidal cells in relation to
937 salinity in gills of Fundulus heteroclitus, a species exhibiting branchial Na+ but not
938 Cl− uptake in freshwater. Cell Tissue Res. 2006;325: 481–492. doi:10.1007/s00441-
939 006-0187-3
940 40. Karnaky KJ, Ernst SA, Philpott CW. Teleost chloride cell. I. Response of pupfish
941 Cyprinodon variegatus gill Na,K-ATPase and chloride cell fine structure to various

high salinity environments. J Cell Biol. 1976;70: 144–156. doi:10.1083/jcb.70.1.144

41. Pisam M, Chrétien M, Rambourg A, Clermont Y. Two anatomical pathways for the renewal of surface glycoproteins in chloride cells of fish gills. Anat Rec. 1983;207: 385–397. doi:10.1002/ar.1092070302

42. Hootman SR, Philpott CW. Accessory cells in teleost branchial epithelium. Am J Physiol-Regul, Integr Comp Physiol. 1980;238: R199–R206. doi:10.1152/ajpregu.1980.238.3.r199

43. Pisam M, Rambourg A. Mitochondria-Rich Cells in the Gill Epithelium of Teleost Fishes: An Ultrastructural Approach. Int Rev Cytol. 1991;130: 191–232. doi:10.1016/s0074-7696(08)61504-1

44. Shiraishi K, Kaneko T, Hasegawa S, Hirano T. Development of multicellular complexes of chloride cells in the yolk-sac membrane of tilapia (Oreochromis mossambicus) embryos and larvae in seawater. Cell Tissue Res. 1997;288: 583–590. doi:10.1007/s004410050844

45. Sardet C, Pisam M, Maetz J. The surface epithelium of teleostean fish gills. Cellular and junctional adaptations of the chloride cell in relation to salt adaptation. J cell Biol. 1979;80: 96–117. doi:10.1083/jcb.80.1.96

46. Karnaky KJ. Structure and Function of the Chloride Cell of Fundulus heteroclitus and Other Teleosts. Am Zoöl. 1986;26: 209–224. doi:10.1093/icb/26.1.209

47. Hiroi J, McCormick SD, Ohtani-Kaneko R, Kaneko T. Functional classification of mitochondrion-rich cells in euryhaline Mozambique tilapia (Oreochromis mossambicus) embryos, by means of triple immunofluorescence staining for Na+/K+-ATPase,Na+/K+/2Cl- cotransporter and CFTR anion channel. J Exp Biol. 2005;208: 2023–2036. doi:10.1242/jeb.01611

48. Inokuchi M, Nakamura M, Miyanishi H, Hiroi J, Kaneko T. Functional

967 classification of gill ionocytes and spatiotemporal changes in their distribution after
968 transfer from seawater to freshwater in Japanese seabass. J Exp Biol. 2017;220:
969 4720–4732. doi:10.1242/jeb.167320
970 49. Hwang P. Multicellular complex of chloride cells in the gills of freshwater
971 teleosts. J Morphol. 1988;196: 15–22. doi:10.1002/jmor.1051960103
972 50. Hsu H-H, Lin L-Y, Tseng Y-C, Horng J-L, Hwang P-P. A new model for fish ion
973 regulation: identification of ionocytes in freshwater- and seawater-acclimated
974 medaka (Oryzias latipes). Cell Tissue Res. 2014;357: 225–243. doi:10.1007/s00441-
975 014-1883-z
976 51. Lunsford ET, Bobkov YV, Ray BC, Liao JC, Strother JA. Anion efflux mediates
977 transduction in the hair cells of the zebrafish lateral line. Proc Natl Acad Sci.
978 2023;120: e2315515120. doi:10.1073/pnas.2315515120
979 52. Cox JPL. Hydrodynamic aspects of fish olfaction. J R Soc Interface. 2008;5:
980 575–593. doi:10.1098/rsif.2007.1281
981 53. Reiten I, Uslu FE, Fore S, Pelgrims R, Ringers C, Verdugo CD, et al. Motile-
982 Cilia-Mediated Flow Improves Sensitivity and Temporal Resolution of Olfactory
983 Computations. Curr Biol. 2017;27: 166–174. doi:10.1016/j.cub.2016.11.036
984 54. Dubaissi E, Papalopulu N. Embryonic frog epidermis: a model for the study of
985 cell-cell interactions in the development of mucociliary disease. Dis Model Mech.
986 2011;4: 179–192. doi:10.1242/dmm.006494
987 55. Yasuda M, Inui T, Hirano S, Asano S, Okazaki T, Inui T, et al. Intracellular Cl−
988 Regulation of Ciliary Beating in Ciliated Human Nasal Epithelial Cells: Frequency
989 and Distance of Ciliary Beating Observed by High-Speed Video Microscopy. Int J
990 Mol Sci. 2020;21: 4052. doi:10.3390/ijms21114052
991 56. Inui T, Murakami K, Yasuda M, Hirano S, Ikeuchi Y, Kogiso H, et al. Ciliary

992 beating amplitude controlled by intracellular Cl− and a high rate of CO2 production in
993 ciliated human nasal epithelial cells. Pflügers Arch - Eur J Physiol. 2019;471: 1127–
994 1142. doi:10.1007/s00424-019-02280-5
995 57. Rao R, Bhalla V, Pastor-Soler NM. Intercalated Cells of the Kidney Collecting
996 Duct in Kidney Physiology. Semin Nephrol. 2019;39: 353–367.
997 doi:10.1016/j.semnephrol.2019.04.005
998 58. Montoro DT, Haber AL, Biton M, Vinarsky V, Lin B, Birket SE, et al. A revised
999 airway epithelial hierarchy includes CFTR-expressing ionocytes. Nature. 2018;560:
1000 319–324. doi:10.1038/s41586-018-0393-7
1001 59. Yuan F, Gasser GN, Lemire E, Montoro DT, Jagadeesh K, Zhang Y, et al.
1002 Transgenic ferret models define pulmonary ionocyte diversity and function. Nature.
1003 2023;621: 857–867. doi:10.1038/s41586-023-06549-9
1004 60. Mauduit O, Aure MH, Delcroix V, Basova L, Srivastava A, Umazume T, et al. A
1005 mesenchymal to epithelial switch in Fgf10 expression specifies an evolutionary-
1006 conserved population of ionocytes in salivary glands. Cell Rep. 2022;39: 110663–
1007 110663. doi:10.1016/j.celrep.2022.110663
1008 61. Bautista JL, Cramer NT, Miller CN, Chavez J, Berrios DI, Byrnes LE, et al.
1009 Single-cell transcriptional profiling of human thymic stroma uncovers novel cellular
1010 heterogeneity in the thymic medulla. Nat Commun. 2021;12: 1096.
1011 doi:10.1038/s41467-021-21346-6
1012 62. Lister JA, Robertson CP, Lepage T, Johnson SL, Raible DW. nacre encodes a
1013 zebrafish microphthalmia-related protein that regulates neural-crest-derived pigment
1014 cell fate. Dev Camb Engl. 1999;126: 3757–67.
1015 63. Tsujikawa M, Malicki J. Intraflagellar Transport Genes Are Essential for
1016 Differentiation and Survival of Vertebrate Sensory Neurons. Neuron. 2004;42: 703–

716. doi:10.1016/s0896-6273(04)00268-5

64. Parsons MJ, Pisharath H, Yusuff S, Moore JC, Siekmann AF, Lawson N, et al. Notch-responsive cells initiate the secondary transition in larval zebrafish pancreas. Mech Dev. 2009;126: 898–912. doi:10.1016/j.mod.2009.07.002

65. Lee RTH, Asharani PV, Carney TJ. Basal keratinocytes contribute to all strata of the adult zebrafish epidermis. Hogan B, editor. PloS one. 2014;9: e84858. doi:10.1371/journal.pone.0084858

66. Haas P, Gilmour D. Chemokine Signaling Mediates Self-Organizing Tissue Migration in the Zebrafish Lateral Line. Developmental Cell. 2006;10: 673–680. doi:10.1016/j.devcel.2006.02.019

67. Stuart T, Butler A, Hoffman P, Hafemeister C, Papalexi E, Mauck WM, et al. Comprehensive Integration of Single-Cell Data. Cell. 2019;177: 1888-1902.e21. doi:10.1016/j.cell.2019.05.031

68. Hao Y, Stuart T, Kowalski MH, Choudhary S, Hoffman P, Hartman A, et al. Dictionary learning for integrative, multimodal and scalable single-cell analysis. Nat Biotechnol. 2024;42: 293–304. doi:10.1038/s41587-023-01767-y

69. Hao Y, Hao S, Andersen-Nissen E, Mauck WM, Zheng S, Butler A, et al. Integrated analysis of multimodal single-cell data. Cell. 2021;184: 3573-3587.e29. doi:10.1016/j.cell.2021.04.048

70. Butler A, Hoffman P, Smibert P, Papalexi E, Satija R. Integrating single-cell transcriptomic data across different conditions, technologies, and species. Nat Biotechnol. 2018;36: 411–420. doi:10.1038/nbt.4096

71. Satija R, Farrell JA, Gennert D, Schier AF, Regev A. Spatial reconstruction of single-cell gene expression data. Nat Biotechnol. 2015;33: 495–502. doi:10.1038/nbt.3192

1042 72. Petkova M. Correlative Light and Electron Microscopy in an Intact Larval
1043 Zebrafish. Doctoral dissertation, Harvard University, Graduate School of Arts &
1044 Sciences. 2020.
1045 73. Kasthuri N, Hayworth KJ, Berger DR, Schalek RL, Conchello JA, Knowles-
1046 Barley S, et al. Saturated Reconstruction of a Volume of Neocortex. Cell. 2015;162:
1047 648–661. doi:10.1016/j.cell.2015.06.054
1048 74. Eberle AL, Mikla S, Schalek R, Lichtman J, Tate MLK, Zeidler D. High-
1049 resolution, high-throughput imaging with a multibeam scanning electron microscope.
1050 J Microsc. 2015;259: 114–120. doi:10.1111/jmi.12224
1051 75. Shapson-Coe A, Januszewski M, Berger DR, Pope A, Wu Y, Blakely T, et al. A
1052 petavoxel fragment of human cerebral cortex reconstructed at nanoscale resolution.
1053 Science. 2024;384: eadk4858. doi:10.1126/science.adk4858
1054 76. Januszewski, Blakely M and, Lueckmann T and, Jan-Matthis. SOFIMA: Scalable
1055 Optical Flow-based Image Montaging and Alignment. 2024. Available:
1056 https://doi.org/10.5281/zenodo.10534541
1057 77. Berger DR, Seung HS, Lichtman JW. VAST (Volume Annotation and
1058 Segmentation Tool): Efficient Manual and Semi-Automatic Labeling of Large 3D
1059 Image Stacks. Front Neural Circuits. 2018;12: 88. doi:10.3389/fncir.2018.00088
1060 78. Schindelin J, Arganda-Carreras I, Frise E, Kaynig V, Longair M, Pietzsch T, et
1061 al. Fiji: an open-source platform for biological-image analysis. Nat Methods. 2012;9:
1062 676–682. doi:10.1038/nmeth.2019
1063 79. Schmid B, Schindelin J, Cardona A, Longair M, Heisenberg M. A high-level 3D
1064 visualization API for Java and ImageJ. BMC Bioinform. 2010;11: 274.
1065 doi:10.1186/1471-2105-11-274
1066 80. Cheung KY, Jesuthasan SJ, Baxendale S, Hateren NJ van, Marzo M, Hill CJ, et

1067 al. Olfactory Rod Cells: A Rare Cell Type in the Larval Zebrafish Olfactory Epithelium

1068 With a Large Actin-Rich Apical Projection. Front Physiol. 2021;12: 626080.

1069 doi:10.3389/fphys.2021.626080